On the computation of long period seismograms in a 3-D earth using normal mode based approximations

Barbara Romanowicz, Mark P Panning, Yuancheng Gung, Yann P Capdeville

HAL Id: insu-01400606

https://insu.hal.science/insu-01400606

Submitted on 22 Nov 2016

On the computation of long period seismograms in a 3-D earth using normal mode based approximations

Barbara A. Romanowicz,[1] Mark P. Panning,[2] Yuancheng Gung[3] and Yann Capdeville[4]

[1]*Berkeley Seismological Laboratory, University of California, Berkeley,* CA 94720, *USA. E-mail: barbara@seismo.berkeley.edu*
[2]*Department of Geosciences, Princeton University, Princeton,* NJ 08544, *USA*
[3]*Department of Geosciences, National Taiwan University, Taipei* 10617, *Taiwan*
[4]*Institut de Physique du Globe,* 75252 *Paris, France*

SUMMARY

Tomographic inversions for large-scale structure of the earth's mantle involve a forward modelling step of wave propagation through 3-D heterogeneity. Until now, most investigators have worked in the framework of the simplest theoretical assumptions, namely the infinite frequency 'ray theory' in the case of body wave traveltime inversions, or the 'path-average' approximation (PAVA) to normal mode perturbation theory, in the case of surface waves and long-period waveforms. As interest is shifting to mapping shorter wavelength structures, the need for a more accurate theoretical account of the interaction of seismic waves with mantle heterogeneity, coupled with improvements in path coverage, has been realized.

Here we discuss different levels of approximations used in the context of normal mode perturbation theory, when modelling time domain seismic waveforms. We compare the performance of asymptotic approximations, which collapse the effects of 3-D structure onto the great circle vertical plane: the 1-D PAVA and a 2-D approximation called non-linear asymptotic coupling theory (NACT), which both are zeroth order asymptotic approximations. We then discuss how off-vertical plane effects can be introduced using higher order asymptotics. These computationally efficient approximations are compared to the linear Born formalism (BORN), which computes scattering integrals over the entire surface of the sphere. We point out some limitations of this linear formalism in the case of spatially extended anomalies, and show how that can be remedied through the introduction of a non-linear term (NBORN). All these approximations are referenced to a precise 3-D numerical computation afforded by the spectral element method. We discuss simple geometries, and explore a range of sizes of anomalies compared to the wavelength of the seismic waves considered, thus illustrating the range of validity and limitations of the various approximations considered.

Key words: Surface waves and free ascillations; Seismic tomography; Theoretical seismology; Wave propagation.

1 INTRODUCTION

Global seismic tomography involves an important forward modelling step, where 3-D model predictions are compared to observables, such as traveltimes of body waves, surface wave dispersion, normal mode spectra or time domain waveforms. It is the difference between observations and predictions that forms the data vector, on the right-hand side of the linearized inversion equation. While other factors come into play, such as data coverage, model parametrization (e.g. which physical parameters to consider?) and mathematical description of the model (e.g. blocks, local or global basis functions), the quality of the 3-D model obtained depends, importantly, on the validity of the approximations that are used in the forward computation step.

Until now, most investigators have relied on very simple, 'zeroth order', theoretical assumptions, such as infinite frequency ray theory in the case of body wave traveltimes, or the 'path-average' approximation (PAVA) in the case of surface waves and long period waveforms. The advantage of these approaches is that they are computationally very fast. They have served several generations of seismic tomography efforts well, revealing first order features of mantle 3-D structure: for example, modelling based on *P*-wave traveltimes has provided images of the deep structure of subduction zones, whereas the two lower mantle broad low velocity regions often referred to as 'superplumes' were characterized through modelling based on a combination of long period *S* phases, normal modes and surface waves (for a review, see Romanowicz 2003). As interest has shifted to mapping shorter wavelength details (e.g. do hot spots

GJI Seismology

plumes originate at the base of the mantle?), the need for a more accurate theoretical treatment of the interaction of seismic waves with mantle heterogeneity has been realized.

Investigators have approached this from two different directions: on the long-period end, where the theoretical framework is generally that of normal mode theory, coupled mode formalisms and asymptotic approximations have been considered, while on the short-period end, where traveltimes of first arrivals are the centrepiece, finite frequency kernels have recently been introduced and discussed extensively (e.g. Dahlen *et al.* 2000; Nolet & Dahlen 2000; Zhao *et al.* 2000; Montelli *et al.* 2004; Zhou *et al.* 2004; Takeuchi 2007). Here we will focus on the goal of modelling long period time domain seismograms containing both body wave and surface wave phases, arguing that the modelling of complete broadband seismograms, with interfering phases of different amplitudes, is the ultimate objective of the next generations of tomographic studies. The richness of phases with different paths in the mantle provides coverage which compensates, to some extent, for the lack of stations in some areas of the world, in particular, in the oceans (e.g. Romanowicz 2008). Clearly, theoretical improvements need to go hand in hand with efforts to fill gaps in the distribution of broad-band stations worldwide (e.g. Trampert & Spetzler 2006).

Until quite recently, an exact method for forward computation of long period seismograms in a 3-D earth containing heterogeneity of arbitrary wavelength was not available. This is now possible owing to the development of powerful numerical methods such as the spectral element method (SEM) and its application to global seismology (Komatitsch & Vilotte 1998; Komatitsch & Tromp 1999). While this approach is revolutionizing seismology, it remains very heavy computationally, and its use for global tomography is still in the developing stages (e.g. Tromp *et al.* 2005; Lekic & Romanowicz 2007). For example, it currently takes ∼4 hr to compute the global wavefield for one event down to 60 s on a modest 32 cpu cluster, while the entire forward part of the waveform modelling can be achieved in that amount of time for 100 events using the PAVA. While clusters are becoming cheaper and faster every day, the next generation of global tomographic models will continue to rely, at least partially, on approximations that render the computation of several iterations of inversion feasible on modest size computers.

There is however, a powerful use that can be made of the SEM capabilities: by comparison of the exact computations with approximate ones, we can (1) test the limits of validity of various approximations and (2) gain physical insight on the role of successive terms in these approximations.

In this paper, we focus on first order perturbation theory, in the context of a normal mode formalism, and its asymptotic approximations. While the basic formalism was developed more than 20 yr ago (e.g. Woodhouse & Dahlen 1978; Woodhouse & Girnius 1982; Woodhouse & Dziewonski 1984), we focus here on zeroth- and higher-order asymptotic approximations and compare them to the full Born approximation. We give in the Appendix the complete higher order asymptotic expressions that we use in the context of modelling elastic effects on the amplitudes (e.g. Romanowicz 1987), such as are important for the retrieval of 3-D anelastic structure of the mantle (e.g. Gung & Romanowicz 2004; Dalton & Ekström 2006).

In what follows, we lead the reader through the different stages of approximations to normal mode perturbation theory that are commonly—or occasionally—used in global mantle tomography, starting with the zeroth order, most standard ones and progressively adding complexity. By comparing approximate and 'exact' synthetic seismograms on some simple examples of structure, we illustrate

the physical meaning of the successive approximations and discuss their limitations. We restrict our exercise to relatively long periods, longer than are used in practice in real inversions, as the main goal is to emphasize the physics of the interaction of seismic waves with heterogeneity.

2 THEORETICAL FRAMEWORK

Here, we compare various levels of asymptotic approximations in the framework of first-order perturbation theory of normal modes. The long period displacement u in a slightly aspherical earth is a solution of the equation (e.g. Woodhouse 1983):

$$(\mathbf{H} + \rho \partial_t^2)\mathbf{u} = \mathbf{f}, \tag{1}$$

where ∂_t denotes partial differentiation with respect to time, $\mathbf{H}$ is the integro-differential operator representing the elastic and gravitational effects, ρ is the density distribution and $\mathbf{f} = \mathbf{f}(\mathbf{x}, t)$ is the body force equivalent of the seismic source.

In the reference spherical, non-rotating, elastic and isotropic (SNREI) model, the corresponding equation is:

$$(\mathbf{H_0} + \rho_0 \partial_t^2)\mathbf{u_0} = \mathbf{f}. \tag{2}$$

The solution can be expanded in terms of the free oscillations $|k>$ of the reference model, which are orthogonal in the sense:

$$\langle k|\rho_0|k'\rangle = \int_V |k>^* \cdot \rho_0|k' > \, dv = \delta_{ij}, \tag{3}$$

where the integration is over the volume of the Earth V, and the asterisk (∗) indicates complex conjugation.

Using the notations of Woodhouse & Girnius (1982), the acceleration $u_0(t)$ in the SNREI reference earth model can be written as:

$$u_0(t) = \mathbf{Re} \sum_k \exp\left[(i\omega_k - \alpha_k)t\right] \sum_m R_k^m S_k^m. \tag{4}$$

Here the sum is taken over all multiplets $|k>$, described by three integers: (n, l, m), where n is the radial order, l the angular order and m the azimuthal order ($|m| < = l$). In an SNREI earth, multiplets are 'degenerate' and for a given n, the corresponding $2l + 1$ singlets all have the same eigenfrequency $\omega_k = {}_n\omega_l$. The complex degenerate frequency of multiplet k is $\omega_k + i\alpha_k$, where α_k accounts for anelastic attenuation. From now on, we will omit the imaginary part of the eigenfrequency, which can be included in the equations when considering anelastic attenuation, invoking the correspondence principle. R_k^m and S_k^m are receiver and source vectors, respectively, which can be written in the form (Woodhouse & Girnius 1982):

$$R_k^m(\theta_r, \phi_r) = \sum_{N=-1}^{N=1} R_{kN} Y_l^{Nm}(\theta_r, \phi_r)$$

$$S_k^m(\theta_s, \phi_s) = \sum_{M=-2}^{M=2} S_{kM} Y_l^{Mm}(\theta_s, \phi_s), \tag{5}$$

where Y_l^{Nm} are the generalized spherical harmonics of Phinney & Burridge (1972), (θ_r, ϕ_r), (θ_s, ϕ_s) are the receiver and source coordinates, respectively, and R_{kN}, S_{kM} are linear combinations of moment tensor elements and spherical earth eigenfunctions, and are given in table 1 of Woodhouse & Girnius (1982).

While higher order normal mode perturbation theory for an aspherical earth has been developed and tested (e.g. Lognonné & Romanowicz 1990; Lognonné 1991; Clévédé & Lognonné 1996;

Clévédé *et al.* 2000), we will limit ourselves here to first order perturbation theory. In this framework, the expression for the acceleration $u(t)$ in a perturbed earth model is (Woodhouse 1983; Li & Tanimoto 1993):

$$u(t) = \mathbf{Re} \sum_{k,k'} \sum_{m,m'} R_k^m \left\{ \exp\left[it\left(\omega_k \delta_{kk'} + \frac{Z_{kk'}^{mm'}}{(\omega_k + \omega_{k'})}\right)\right] \right.$$
$$\left. - \exp(i\omega_k t) P_{kk'}^{mm'} \right\} S_{k'}^{m'}, \tag{6}$$

where

$$Z_{kk'}^{mm'} = H_{kk'}^{mm'} - \omega^2 P_{kk'}^{mm'}. \tag{7}$$

Here k, k' denote two multiplets and m, m' are the azimuthal orders of singlets within each of these multiplets, and the effect of lateral heterogeneity is expressed through the splitting matrix elements:

$$H_{kk'}^{mm'} = H_{ij} = \langle i|H|j \rangle = \int_V |i >^* H|j > \, dV$$

$$P_{kk'}^{mm'} = P_{ij} = \langle i|\delta\rho|j \rangle = \int_V |i >^* \delta\rho|j > \, dV. \tag{8}$$

It is common practice to neglect the term in $P_{kk'}$ in expression (6), as it is a small amplitude perturbation due to density heterogeneity and it does not evolve with time (it is different from the amplitude perturbation due to focusing effects).

A convenient expression for $Z_{kk'}$ can be obtained by introducing the local frequency shift $\delta\omega_{kk'}$ resulting from coupling of multiplets (k, k') by heterogeneity, defined in terms of model perturbations at a position (θ, ϕ) on the earth's surface, as follows:

$$\delta\omega_{kk'}(\theta, \phi) = \frac{1}{2\omega_{kk'}} \left[\int_0^a \delta\mathbf{m}(r, \theta, \phi) \cdot \mathbf{M}_{kk'}(r) r^2 dr \right]$$
$$- \left[\sum_d r_d^2 h_d(\theta, \phi) H_{kk'}^d \right], \tag{9}$$

where $\omega_{kk'} = (\omega_k + \omega_{k'})/2$. For volumetric heterogeneity, the model perturbation vector at point (r, θ, ϕ) in the Earth is $\delta\mathbf{m}(r, \theta, \phi)$. $\mathbf{M}_{kk'}(r)$ is the corresponding kernel vector, and the integral is taken over radius r from the centre of the earth to its surface at radius a. Likewise, $h_d(\theta, \phi)$ is the perturbation to the position of discontinuity d beneath the point (θ, ϕ), and $H_{kk'}^d$ is the corresponding kernel. For completeness, perturbations due to rotation should be added to eq. (9), as given by Dahlen (1968) and Woodhouse & Dahlen (1978). In the isotropic case, expressions for the kernels in eq. (9) have been derived by Woodhouse & Dahlen (1978) in the case of self-coupling ($k = k'$), and extended by Romanowicz (1987) to the case of coupling between different multiplets. Li & Romanowicz (1996) give the corresponding expressions in the case of a radially anisotropic model and other authors provide the means to compute them in the general anisotropic case (Mochizuki 1986a; Tanimoto 1986; Romanowicz & Snieder 1988).

As shown in Woodhouse & Girnius (1982) for the self-coupling case, and in Romanowicz (1987) and Romanowicz & Snieder (1988) in a more general case:

$$Z_{kk'}^{mm'} = \sum_{i=0}^{i=2} \omega_{kk'} \iint_\Omega \delta\omega_{kk'}(\theta, \phi)(-\nabla^2)^i \left[Y_l^{m*}(\theta, \phi) Y_{l'}^{m'}(\theta, \phi) \right] d\Omega, \tag{10}$$

where integration is over the unit sphere Ω. Going back to eq. (6), we thus obtain (e.g. Li & Tanimoto 1993):

$$u(t) = \mathbf{Re} \sum_{ij} R_i \exp\left\{ i\left[\omega_i \delta_{ij} + \frac{Z_{ij}}{(\omega_i + \omega_j)}\right] t \right\} S_j, \tag{11}$$

where $i = (k, m)$ and $j = (k', m')$ are two individual singlets, and R_i and S_j are the corresponding receiver and source vectors.

We note that expression (11) is uniformly valid at all times (Li & Tanimoto 1993), that is, no short-term approximation has been made yet.

In the 'self-coupling' case, which is widely used in the context of normal mode data analysis, such as, for example, in the determination of mode splitting functions (e.g. Giardini *et al.* 1988; Li *et al.* 1991), the sum is restricted to coupling of singlets within the same multiplet, and expression (11) becomes:

$$u(t) = \mathbf{Re} \sum_k \sum_{mm'} R_k^m \exp\left[i\left(\omega_k + \frac{Z_{kk}^{mm'}}{2\omega_k}\right) t \right] S_k^{m'}. \tag{12}$$

A convenient intermediate observable in this case is the 'splitting function' (Giardini *et al.* 1988):

$$\gamma(\theta, \phi) = \sum_{st} c_s^t Y_s^t(\theta, \phi). \tag{13}$$

The splitting coefficients c_s^t's are defined through:

$$Z_{kk}^{mm'} = \omega_0 \sum_{s=0}^{s=2l} \sum_{l=-s}^{l=+s} \gamma_{ls}^{mm't} c_s^t + m\Omega\beta\delta_{mm'}, \tag{14}$$

where the second term represents the effect of rotation [Ω is the rate of rotation of the earth and β the rotation splitting parameter (Dahlen 1968)]. Also

$$c_s^t = \int_0^a \delta m_{st}(r) \mathbf{M}_{ss}(r) r^2 dr + \sum_d \delta h_{st}^d \mathbf{H}_{ss}^d. \tag{15}$$

Here $\delta m_{st}(r)$ is a spherical harmonics coefficient of degree and order (s, t) of the model pertubation at radius r, and:

$$\gamma_{ls}^{mm't} = \int_0^{2\pi} \int_0^{2\pi} Y_l^{m*}(\theta, \phi) Y_s^t(\theta, \phi) Y_l^{m'}(\theta, \phi) \sin(\theta) \, d\theta \, d\phi. \tag{16}$$

In this approximation, it can be shown that the seismogram depends only on even order heterogeneity, that is, it is incomplete for the purpose of study of Earth's 3-D structure (e.g. Romanowicz & Roult 1986). For normal mode analysis, however, it is a reasonably good first order approximation, given that a propagating seismic wave travels many times around the great circle to form a standing mode, and is therefore primarily sensitive to structure that is symmetric with respect to the centre of the earth. However, the terms arising from coupling between different multiplets need to be included to recover sensitivity to the odd terms of the 3-D structure. Linearized expressions for the perturbation to the seismogram, convenient for the study of mode coupling can be found in Giardini *et al.* (1988) and have been used to obtain some information on odd structure from the analysis of mode splitting (e.g. Resovsky & Ritzwoller 1995; Durek & Romanowicz 1999; Kuo & Romanowicz 2002; Andrews *et al.* 2006).

When the focus is not the study of normal modes but that of long period seismograms in the time domain or traveltimes of seismic phases, as in most studies based on the first order Born approximation, expression (11) is linearized, assuming short times [$t \ll 2\pi ||Z_{ij}/(\omega_i + \omega_j)||^{-1}$], so that the acceleration seismogram then becomes:

$$u(t) = u_0(t) + \delta u(t) \tag{17}$$

with

$$\delta u(t) = \mathbf{Re} \sum_{kk'} \frac{\exp(i\omega_k t) - \exp(i\omega_{k'} t)}{\omega_k^2 - \omega_{k'}^2} \times A_{kk'}, \tag{18}$$

where

$$A_{kk'} = \sum_{mm'} R_k^m Z_{kk'}^{mm'} S_{k'}^{m'}. \tag{19}$$

Using eq. (10) and the addition theorem for spherical harmonics, $A_{kk'}$ can be written in the form (Romanowicz 1987; Li & Tanimoto 1993)

$$A_{kk'} = \mathbf{Op_1 Op_2} \int \int_\Omega \delta\omega_{kk'} Y_l^0(\lambda) Y_{l'}^0(\beta)\, d\Omega, \tag{20}$$

where $\mathbf{Op}_1$ and $\mathbf{Op}_2$ are two linear differential operators acting on the epicentral and station coordinates, respectively. We see that the computation of the scattering term (20) involves integration over the surface of the whole sphere.

The linearization in eq. (18) introduces a secular term, indeed:

$$\sum_{kk'} \frac{\exp(i\omega_k t) - \exp(i\omega_{k'} t)}{\omega_k^2 - \omega_{k'}^2} A_{kk'}$$
$$= \sum_k \left[\sum_{k'=k} \frac{it}{2\omega_k} A_{kk} + \sum_{k' \neq k} \frac{\exp(i\omega_k t)}{\omega_k^2 - \omega_{k'}^2} (A_{kk'} + A_{k'k}) \right]. \tag{21}$$

The first term in eq. (21) represents coupling within the multiplet k (otherwise known as 'self-coupling'), the second term represents coupling between multiplet k and all other multiplets.

When both terms in eq. (21) are considered, we obtain the first Born approximation (BORN), and the perturbation to the seismogram (eq. 18) becomes (Woodhouse 1983; Tanimoto 1984):

$$\delta u(t) = \mathbf{Re} \sum_k \left[\sum_k \frac{it}{2\omega_k} \sum_{mm'} R_k^m H_{kk}^{mm'} S_k^{m'} \right.$$
$$\left. + \sum_{k' \neq k} \frac{\exp(i\omega_k t)}{\omega_k^2 - \omega_{k'}^2} \times \sum_{mm'} R_k^m Z_{kk'}^{mm'} S_{k'}^{m'} \right]. \tag{22}$$

This approximation is the basis for the 'finite-frequency' theory leading to the 'banana–doughnut' kernels. From eq. (10), we see that the computation of the perturbation to the seismograms involves an integration over the whole sphere of the local frequencies of all the modes considered. This is heavy computationally, while valid only for weak heterogeneity (single scattering) and short times (the linear term in t). In fact, the Princeton body wave approach does not use a mode formalism in the calculation of the kernels, but decreases the computational burden by using a paraxial far-field ray approximation to more quickly determine the value of the integrand in the Born approximation. This speed-up, of course, comes at the cost of retaining some shortcomings of ray theory, in particular the inability to model diffracted phases.

To avoid the drawbacks of the short time approximation, we can linearize eq. (11) differently, as was done in Li & Romanowicz (1995), by replacing ω_i and Z_{ij} by:

$$\tilde{\omega}_i = \omega_i + \delta\tilde{\omega}_i$$
$$\tilde{Z}_{ij} = Z_{ij} - 2\omega_i \delta\tilde{\omega}_i \delta_{ij}, \tag{23}$$

where we define the frequency shift $\delta\tilde{\omega}_i$ as:

$$\delta\tilde{\omega}_i = \frac{1}{\Delta} \int_S^R \delta\omega_i(s)\, ds \tag{24}$$

and the integral is taken along the great circle path.

The perturbed seismogram can then be written:

$$u(t) = \sum_k A_k \exp(i\tilde{\omega}_k t) + \delta u(t) \tag{25}$$

with

$$A_k = \sum_m R_k^m S_k^m$$
$$\delta u(t) = -\sum_k it\delta\tilde{\omega}_k A_k \exp(i\tilde{\omega}_k t) + \sum_k \sum_{k' C \Gamma_k} D_{kk'}(t) A_{kk'}, \tag{26}$$

where Γ_k is the set of multiplets whose eigenfrequencies are higher than or equal to ω_k, and (e.g. Li & Romanowicz 1995), and:

$$D_{kk'}(t) = \frac{\exp(i\tilde{\omega}_k t) - \exp(i\tilde{\omega}_{k'} t)}{(\omega_k + \omega_{k'})(\tilde{\omega}_k + \tilde{\omega}_{k'})} \tag{27}$$

The definition of $\delta\tilde{\omega}_k$ is somewhat arbitrary. Instead of the integral along the path from the source to the receiver, one could also choose to define it as the great circle average of the local frequency, which then relates more directly to the expressions introduced by Woodhouse & Dziewonski (1984).

When $A_{kk'}$ in eq. (26) is computed exactly, the non-linear expression (25) represents a modification to the single scattering Born approximation (eq. 22). It includes multiple forward scattering, which is a better approximation in the case of long paths across relatively homogeneous structure, such as defined by the long wavelength part of the model (e.g. Panning *et al.* 2008). We call this modified Born approximation 'non-linear Born formalism' (NBORN). We note that these scattering integrals are computationally very heavy.

When the wavelength of the elastic wave is short compared to the wavelength of structure, the sensitivity of the wave is concentrated along the great circle, and asymptotic approximations to the Legendre functions give quite accurate results, away from the source, the receiver and their antipodes. We will now consider these asymptotic expressions.

2.1 Asymptotic approximations

The integrals over the sphere are computationally time consuming, especially as there are many modes to couple, however, at angular orders l corresponding to wavelengths large compared to those of lateral heterogeneity, it is possible to replace the expressions for the spherical harmonics Y_l^{NM} by their asymptotic approximations, derived from those of the generalized Legendre polynomial P_l^{NM}, which is, to order $1/l$:

$$k_l P_l^{MN}(x) = \frac{1}{\pi\sqrt{\sin\Delta}} \cos\left[kx + \frac{(N+M)\pi}{2} - \frac{\pi}{4} + \frac{1}{k}\alpha_{NM}(x) \right]$$
$$+ O\left(\frac{1}{l^2}\right), \tag{28}$$

where

$$\alpha_{NM}(x) = \left[\frac{(N^2 + M^2)}{2} - \frac{1}{8} \right] \cot x - \frac{MN}{\sin x} \tag{29}$$

and

$$k_l = \sqrt{\frac{2l+1}{4\pi}}. \tag{30}$$

We can express $A_{kk'}$ (eq. 19) in terms of generalized Legendre polynomials (e.g. Li & Tanimoto 1993)

$$A_{kk'} = \sum_N \sum_M R_{kN} S_{k'M} \int_\Omega \delta\omega_{kk'}^2 X_l^{N0}(\beta) X_{l'}^{M0}(\lambda)$$
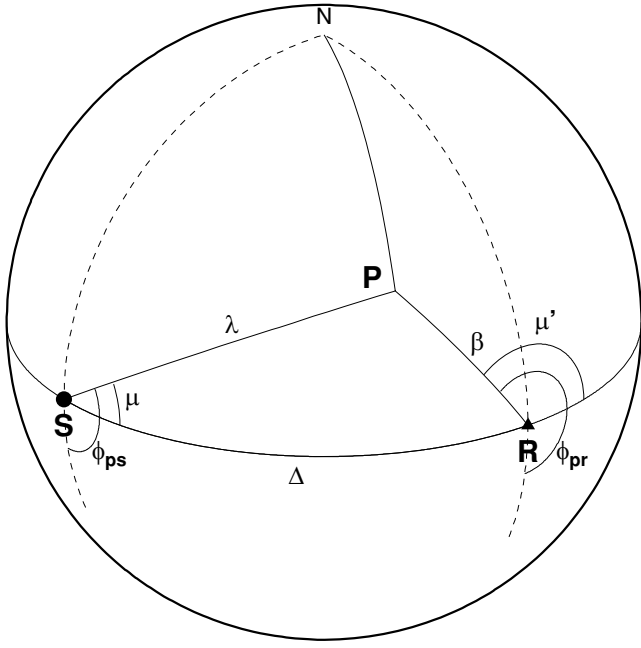$$\times \exp\left[i\left(M\Phi_{ps} - N\Phi_{pr}\right) \right] d\Omega, \tag{31}$$

Figure 1. Source–receiver geometry and definition of angles used in the text.

where, if P_l^N, $P_{l'}^M$ are associated Legendre functions, the normalization is such that:

$$X_l^{N0} = k_l P_l^N. \tag{32}$$

The angles λ, β, Φ_{ps} and Φ_{pr} are defined in Fig. 1, and

$$\delta\omega_{kk'}^2 = 2\omega_{kk'}\delta\omega_{kk'}. \tag{33}$$

2.1.1 Self-coupling

Introducing the 'location parameter' (Jordan 1978) corresponding to multiplet k

$$\Lambda_k = \frac{\sum_{mm'} R_k^m Z_{kk}^{mm'} S_k^{m'}}{\sum_{mm'} R_k^m S_k^{m'}} \tag{34}$$

the self-coupling seismogram (eq. 12) can be written as:

$$u(t) = \mathbf{Re} \sum_k \sum_{mm'} R_k^m S_k^{m'} \exp[i(\omega_k + \Lambda_k)t]. \tag{35}$$

It can be shown that, asymptotically (Jordan 1978; Romanowicz & Roult 1986)

$$\Lambda_k = \delta\hat{\omega}_k + O(1/l), \tag{36}$$

where $\delta\hat{\omega}_k$ is the great circle average of the local frequency $\delta\omega_k(\theta, \phi)$ corresponding to multiplet k

$$\delta\hat{\omega}_k = \frac{1}{2\pi} \int_\Omega \delta\omega_k(\theta, \phi)\, d\Omega. \tag{37}$$

Thus, for high enough frequencies and correspondingly smooth earth models, the effect of lateral heterogeneity on multiplet k is a frequency shift $\delta\hat{\omega}_k$ which depends only on the average structure beneath the great circle containing the source and the station. This allowed Masters *et al.* (1982) to meaningfully plot these frequency shifts as a function of position of the poles of the corresponding great circles, and discover the now well known 'degree two pattern' originating in the upper-mantle transition zone.

2.1.2 Complete first-order seismograms

Let us now consider complete seismograms and first discuss the asymptotic approximation of order zero in $1/l$. We will distinguish two cases.

(i) Along branch coupling only, in which we do not consider coupling across different mode branches, that is, we only couple modes which have the same overtone number n.

(ii) Coupling both along and across mode branches.

2.1.3 The 'path average' approximation

Case (i) was studied by Mochizuki (1986b) and Romanowicz (1987), who showed that, by applying the stationary phase approximation to order zero, this leads to the so-called PAVA of surface wave analysis, accounting for the effect of structure along the minor arc.

Following the notations of Romanowicz (1987), we define the displacement operator $\mathbf{D}$, the projection on a given component of motion $\mathbf{v}$, the strain tensor operator $\boldsymbol{\epsilon}$ and the source moment tensor $\mathbf{M}$. $\boldsymbol{\epsilon}$ and $\mathbf{D}$, here considered in the spherical earth, depend on the multiplet [i.e. on the integers (n, l)] but not on the azimuthal order m. Therefore, for multiplet k, we can write, in operator notation:

$$\sum_{mm'} R_k^m S_k^{m'} = (\mathbf{v} \cdot \mathbf{D})(\epsilon : \mathbf{M})\left[\sum_{mm'} Y_l^m(\theta_s)^* Y_l^{m'}(\theta_r)\right]$$
$$= (\mathbf{v} \cdot \mathbf{D})(\epsilon : \mathbf{M}) k_l Y_l^0(\Delta), \tag{38}$$

where Δ is the epicentral distance, and we have applied the summation rule for spherical harmonics, since the operators depend only on l and n, not on m. Let:

$$A_0^k(\Delta) = (\mathbf{v} \cdot \mathbf{D})(\epsilon : \mathbf{M}) k_l Y_l^0(\Delta). \tag{39}$$

The spherical earth seismogram is then:

$$u_o(t) = \mathbf{Re} \sum_k A_0^k(\Delta) e^{i\omega_k t}. \tag{40}$$

It can be shown (e.g. Romanowicz 1987) that self-coupling combined with along-branch coupling yield the following expression for the seismogram, asymptotically, to order zero in $1/l$:

$$u_{\text{pava}}(\theta_r, \phi_r, t) = \sum_k A_k^0(\Delta + \delta\Delta) \exp[i(\omega_k + \delta\hat{\omega}_k)t], \tag{41}$$

where

$$\delta\Delta = \frac{a\Delta}{U(l + 1/2)}(\delta\hat{\omega}_k - \delta\tilde{\omega}_k). \tag{42}$$

Here $\delta\hat{\omega}_k$ is the great circle average frequency defined in eq. (37), $\delta\tilde{\omega}_k$ is the 'minor arc average', defined in eq. (24):

We thus see that along-branch coupling is necessary to describe the sensitivity of the seismogram to odd-order heterogeneity, namely heterogeneity that is not symmetric with respect to the centre of the earth (i.e. perturbation along the minor arc). Expression (41) is identical to that posited by Woodhouse & Dziewonski (1984) for the modelling of waveforms in a 3-D earth with both even and odd order heterogeneities.

We note that in the PAVA approximation, the seismogram is sensitive only to the average structure between the source and the receiver and along the great circle path, that is, the corresponding sensitivity kernels are '1-D' in the vertical plane containing the source and the receiver. This approximation is best for single-mode seismograms, such as fundamental mode surface waves. The equivalence of the

time domain expression (41) with the standard phase velocity measurements of single mode surface waves in the frequency domain was demonstrated in Romanowicz (1987).

The next step in complexity is the introduction of 'across branch coupling', to order zero in $(1/l)$.

2.1.4 Across-branch coupling

The PAVA approximation is not a good approximation for body waves, whose sensitivity is concentrated along the ray theoretical ray path. It is also not well suited for surface wave overtones, which are formed by interactions of body waves. As shown by Li & Tanimoto (1993), it is necessary to consider across-branch coupling to correctly describe the ray sensitivity of body waves.

The formalism of Li & Tanimoto (1993) is a purely linear, single scattering formalism. In this case, the seismogram is written:

$$u(t) = u_0(t) + Re \sum_{kk'} \frac{\exp(i\omega_k t) - \exp(i\omega_{k'} t)}{\omega_k^2 - \omega_{k'}^2} A_{kk'}, \qquad (43)$$

where $u_0(t)$ is the reference 1-D seismogram, and $A_{kk'}$ is calculated using the stationary phase approximation to order zero.

While it provides a better representation of the 2-D sensitivity of body waves to structure in the vertical plane containing source and receiver, this formalism has some disadvantages with respect to the time domain PAVA, in which the complete series along the great circle path is included in the exponential term. As already introduced earlier, Li & Romanowicz (1995) proposed a modification (non-linear asymptotic coupling theory, NACT) of the Li & Tanimoto (1993) formalism by re-introducing the path average perturbation in the exponential term, and appropriately removing it from the linearized across-branch coupling term as expressed in eqs (26). The expression for $A_{kk'}$ in eq. (26) (eq. 13 of Li & Romanowicz 1995) is:

$$A_{kk'} = \frac{1}{2\pi} \left[Q_{kk'}^{(1)} \int_0^{2\pi} \delta\omega_{kk'}^2 \cos j\phi \, d\phi + Q_{kk'}^{(2)} \int_0^{2\pi} \delta\omega_{kk'}^2 \sin j\phi \, d\phi \right] \qquad (44)$$

here $j = l' - l$ and the source and receiver terms $Q_{kk'}^{(1)}$ and $Q_{kk'}^{(2)}$ are given in appendix A of Li & Romanowicz (1995). Note that this expression is only used for $k'C\Gamma_k$ (across-branch coupling terms).

The NACT approximation provides 2-D sensitivity of the seismogram in the vertical plane containing source and receiver and is thus a better approximation than PAVA to model the propagation of body waves. Moreover, it preserves the long-time validity of the PAVA part of the seismogram.

Neither PAVA nor NACT account for sensitivity outside of the great circle vertical plane, and therefore only allow to accurately model variations in the phase part of the seismogram, as the phase is better behaved than the amplitude and less sensitive to off-great circle effects. In contrast, strong variations in the amplitudes of the waveforms can be observed due to off-great circle focusing/defocusing effects.

2.1.5 Higher-order asymptotics

In order to include the off-great circle path sensitivity in the seismogram, it is necessary to conduct the asymptotic computations to higher order in $(1/l)$. This was shown by Romanowicz (1987) and Park (1987). Romanowicz (1987) gave the expressions for the seismogram for the vertical component of motion. Here we present the general result, with the algebra explicited in the Appendix. It involves using expression (28) for the generalized Legendre polynomials as well as the stationary phase to order $(1/l)$ (as shown in Romanowicz 1987). The expression thus obtained for the order $(1/l)$ contribution δu_k^1 of multiplet k to the seismogram, is:

$$\delta u_k^1(t, \Delta) = \frac{1}{\pi k_l \sqrt{\sin \Delta}} \left[\cos\left(k\Delta - \frac{\pi}{4}\right) \right.$$
$$\times \left(B_0^1 \cos \omega_k t - t B_1^1 \sin \omega_k t \right)$$
$$\left. + \sin\left(k\Delta - \frac{\pi}{4}\right) \left(C_0^1 \cos \omega_k t - t C_1^1 \sin \omega_k t \right) \right], \qquad (45)$$
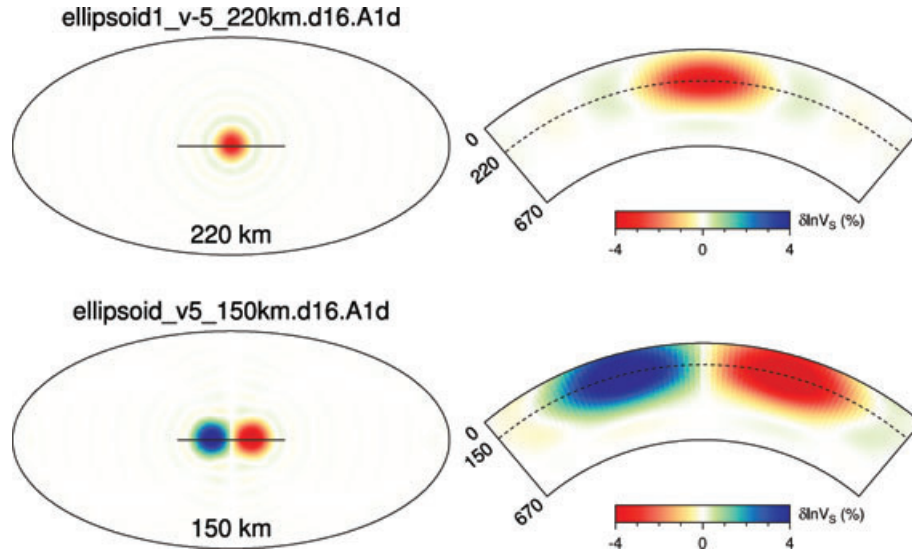

Figure 2. Simple models used in forward calculations. Top panels: single low velocity anomaly (Model 1). Left-hand panel: view from above; Right-hand panel: vertical cross section along the line shown in the left-hand panel. Bottom panels: Same as top for a model with two anomalies of equal amplitude and opposite signs (Model 2). In all cases, the anomalies correspond to a wavelength corresponding to spherical harmonic degree 16 (about 1250 km), and shear wave velocity anomalies of ± 5 per cent.

where

$$B_0^1 = \frac{a\Delta}{lU}(F_1 - \tilde{F}_7) - \frac{F_6}{l}$$

$$B_1^1 = \frac{F_4 - \tilde{F}_{10}}{l}$$

$$C_0^1 = -\frac{a\Delta}{lU}(F_2 - \tilde{F}_8) - \frac{F_5}{l} \qquad (46)$$

$$C_1^1 = \frac{F_3 - \tilde{F}_9}{l}$$

and the expressions for $F_0 \dots \tilde{F}_{10}$ are given in the Appendix. This generalizes the expressions of Romanowicz (1987) to any moment tensor source and any component of observation: In eq. (46), the coefficients B_0^1, B_1^1, C_0^1 and C_1^1 depend only on minor arc and great circle averages of the local frequency and its spatial first and second derivatives (in particular, derivatives transverse to the great circle path). As shown by Romanowicz (1987), the expressions obtained for the focusing terms are equivalent to those obtained by Woodhouse & Wong (1985) by ray tracing on the sphere.

As we will show in the next section, this approximation works well for certain epicentral distance ranges, but is more restrictive in its domain of validity than the PAVA/NACT, because of the divergence of the $1/l$ terms.

Note that, in the case where only self-coupling is considered to order $(1/l)$, we obtain the next approximation of the mode frequency shift (e.g. Romanowicz & Roult 1986) or location parameter:

$$\Lambda_k = \delta\hat{\omega}_k + \frac{\hat{D}_k}{8l}\cot(k\Delta - \pi/4) + O(1/l^2), \qquad (47)$$

where $\hat{D}_k$ is the great circle average of the transverse gradient of structure

$$\hat{D}_k = \frac{1}{2\pi}\int_\gamma D_k(s)\mathrm{d}s. \qquad (48)$$

The expression for D_k is given in the Appendix and is the same as that of Woodhouse & Wong (1985) (converted from phase velocity to frequency shift formalism).

This introduces quasi-periodic oscillations around the average frequency shift as a function of angular order as was illustrated in real data by Romanowicz & Roult (1986) and Pollitz *et al.* (1987). Since the $1/l$ term is only the first term of a truncated asymptotic series, the oscillations around the average frequency shift can become divergent at certain combinations of Δ and k, because of the division by $\sin(k\Delta - \pi/4)$, limiting the range of validity of this asymptotic approximation.

3 PRACTICAL EXAMPLES/DISCUSSION

In what follows, we illustrate the effects of the different approximations discussed in the preceding section on simple synthetic examples. Two simple structures embedded in a spherically symmetric Earth will be considered (Fig. 2). The first structure (Model 1) is simply a low velocity anomaly of ellipsoidal shape. The second structure (Model 2) comprises two ellipsoidal anomalies of the same shape, amplitude and position, but of different signs. Three different sources will be considered. An 'isotropic' source, used for the computations with Model 1, and a double couple source for Model 2. The amplitudes and sizes of the anomalies will be varied.

We calculate reference synthetic seismograms for the reference 1-D radially symmetric model, a simplified model based on PREM (Dziewonski & Anderson 1981), but with smoother depth variations

to reduce computation time in SEM, and for the 3-D models defined in Fig. 2. For these calculations, we used the 'coupled' SEM (Capdeville *et al.* 2002; Chaljub *et al.* 2003), down to 100 s period. In this approach, the SEM is used in the mantle, and coupled to a mode computation in the 1-D core. In what follows, comparisons of asymptotic approximations to BORN and NBORN will be presented. The BORN computations are here performed according to the efficient approach described in Capdeville (2005).

3.1 Body wave character: 2-D effects in the vertical plane on overtones

Fig. 3 illustrates the importance of considering 2-D kernels in the vertical plane containing the source and the receiver, when modelling overtones, and more generally body waves. Here we compare 3-D synthetics for a path traversing the two-anomaly structure (Model 2) along its vertical plane of symmetry. The source is a double-couple source located in the plane of symmetry, with a maximum of radiation for Rayleigh waves in the source-station direction.
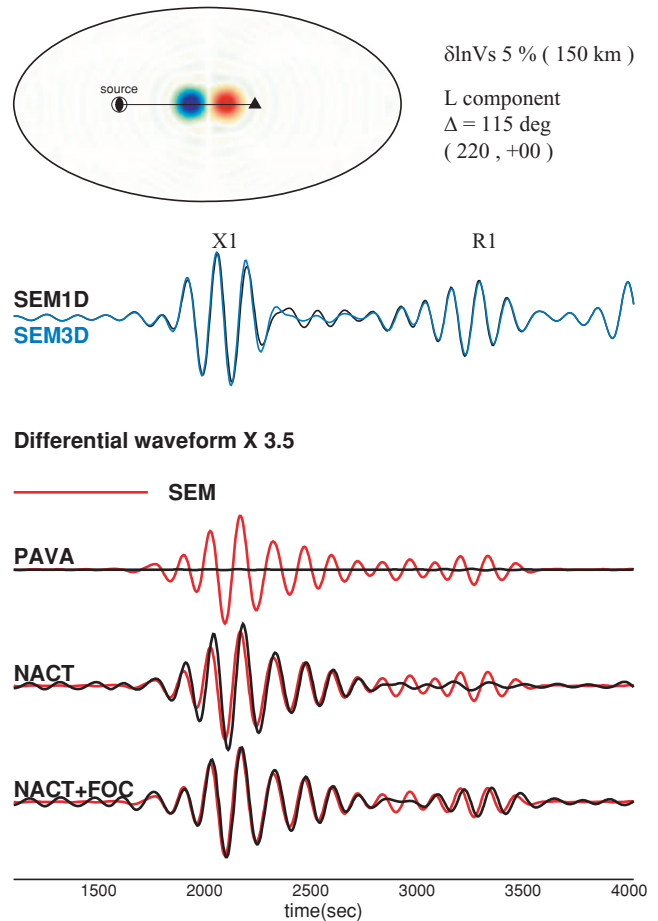

Figure 3. Comparison of synthetic seismograms computed for the radial component, in Model 2 at an epicentral distance of 115°. The source is a double couple 45° dipping north south striking normal fault. The waveforms at the top show a comparison of 1-D and 3-D synthetics computed using C-SEM, down to 100 s period. Below are shown differential waveforms between the 3-D and 1-D calculations, for different approximations (PAVA, NACT, NACT+FOC, shown in red), and for the SEM calculations, shown in black, for reference. In this case, the PAVA approximation performs poorly for the overtone wavepacket X1, because the effect of the two equal and opposite anomalies cancels out.

The reference 3-D seismograms computed using C-SEM, and compared to the 1-D reference seismograms, show a larger difference for the overtone wave train X1 than for the fundamental mode wave train R1. PAVA is not able to reproduce this difference: for PAVA the differential trace is flat, reflecting the fact that PAVA sensitivity is 1-D, and 'sees' only the average structure between the source and the receiver, which has zero anomaly, at any given depth, since the effects of the two anomalies cancel each other.

On the other hand, NACT, with its 2-D kernels, is able to reproduce the 3-D effects on the overtone wave packet quite well,

but does not improve the fit for the fundamental mode. The remaining very small misfit in the overtones, and much of the fundamental mode misfit can be explained by focusing effects (i.e. off path propagation) and the asymptotic focusing computation (NACT+FOC) does a good job in this case, except for a small portion of the time-series between X1 and R1, likely due to the truncation in the number of modes that are considered for the coupling computation.

This example shows that, for the modelling of overtones at low frequency, the most important effect is the 2-D effect in the vertical
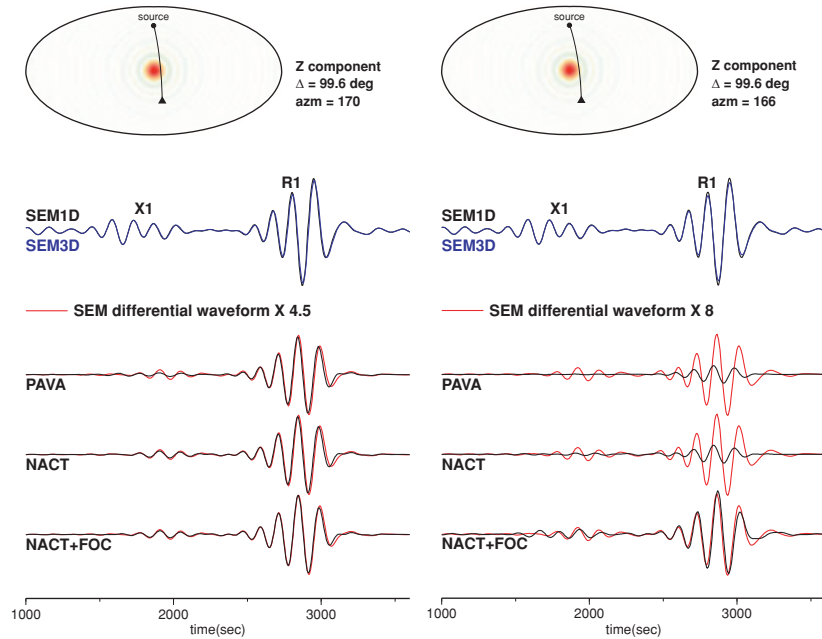

Figure 4. Comparison of synthetic seismograms computed for the vertical component, in Model 1 at an epicentral distance of 99.6°, for an isotropic source. As in Fig. 3, the waveforms at the top show a comparison of 1-D and 3-D synthetics computed using C-SEM, down to 100 s period. Below are shown differential waveforms between the 3-D and 1-D calculations, for different approximations (PAVA, NACT, NACT+FOC, shown in red), and for the SEM calculations, shown in black. Left-hand panel: computation at an azimuth of 170° from North, in which the path penetrates into the anomaly. All approximations perform well in this case. Right-hand panel: computation at an azimuth of 166°, in which the ray grazes the anomaly. In this case neither PAVA, nor NACT are able to match the SEM computations. It is necessary to introduce off-plane effects (NACT+FOC).
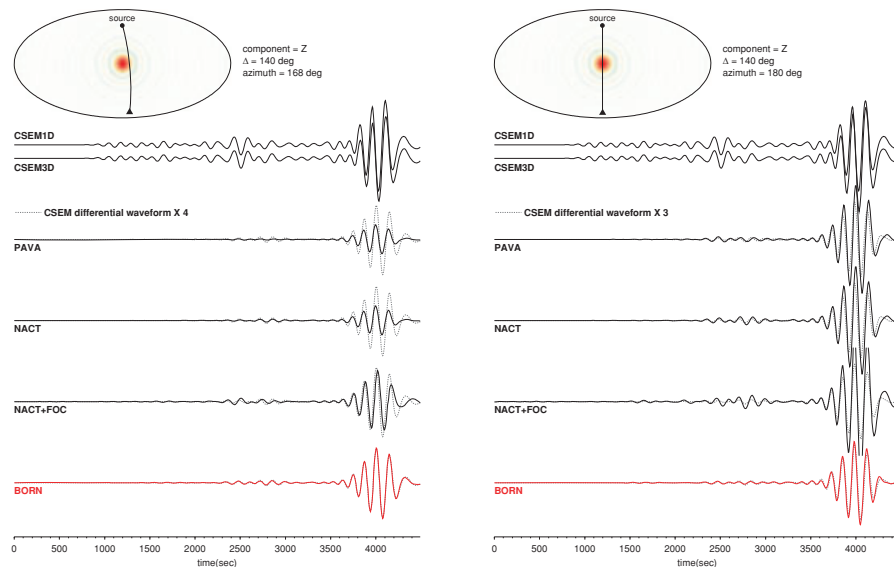

Figure 5. Same as Fig. 4, but for a distance of 140°, and azimuths of 168° (left-hand panel) and 180° (right-hand panel), also showing a comparison with the linear BORN computation. In this case, the linear Born computation gives the most satisfactory fits to the SEM computation.
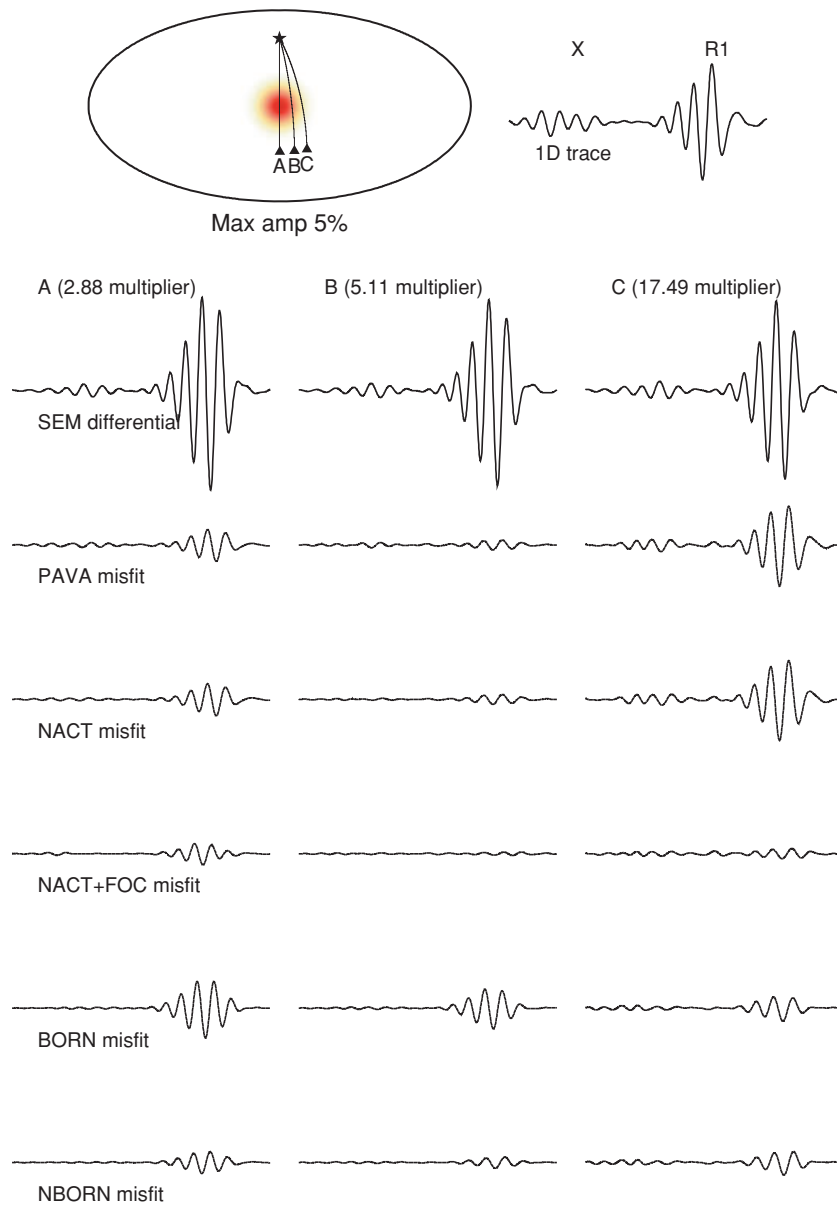
Figure 6. (a) Comparison of synthetic seismograms for a Model 1 anomaly of larger size (diameter 22.5°, or ~2500 km), using different approximations and for different azimuths. (A) azimuth of 180°; (B) azimuth of 168° and (C) azimuth of 160°. In the top plot, the star denotes the location of the source, and the triangles are stations for which waveforms are shown. Here we show only the 1-D trace (top right-hand panel), the 3D–1D differential seismograms (second row), and misfits between the 3-D SEM computation and the various approximations. In addition to PAVA, NACT, NACT+FOC and linear BORN, where also show the comparison with NBORN. In this case, the linear BORN approximation behaves poorly and the NBORN modification improves the fit to SEM. However, for paths B and C, the asymptotic NACT+FOC approximation provides slightly better fits than NBORN. Here and in the following figures the anomalies are defined as Gaussian anomalies of given diameter. The multiplier at the top of each column is applied to the differential trace and all the misfit traces in that column, which are relative to the 1-D trace plotted at the top right-hand corner of the figure. (b) Same as (a) for the case of a smaller wavelength anomaly, one of full width half maximum size 5°.

plane. The focusing effects are of second order for such smooth structures.

3.2 Focusing effects: 2-D effects in the horizontal plane

In Fig. 4, we consider the single slow anomaly model (Model 1) and paths grazing the anomaly at different azimuths from an isotropic source located on a symmetry plane north of the anomaly. In the left-hand panel, the path very slightly penetrates into the anomaly. The PAVA approximation works well in this case and is able to explain most of the difference between 1-D and 3-D seismograms, particularly for the fundamental mode, which is here the strongest phase and is well isolated from overtones. In the right-hand panel of Fig. 4, on the other hand, the path is slightly further away from the anomaly. In this case, PAVA is not able to explain the 3-D effects on the R1 waveform, and NACT does not help. Introducing focusing effects turns out to be crucial to explain the 3-D waveforms both for
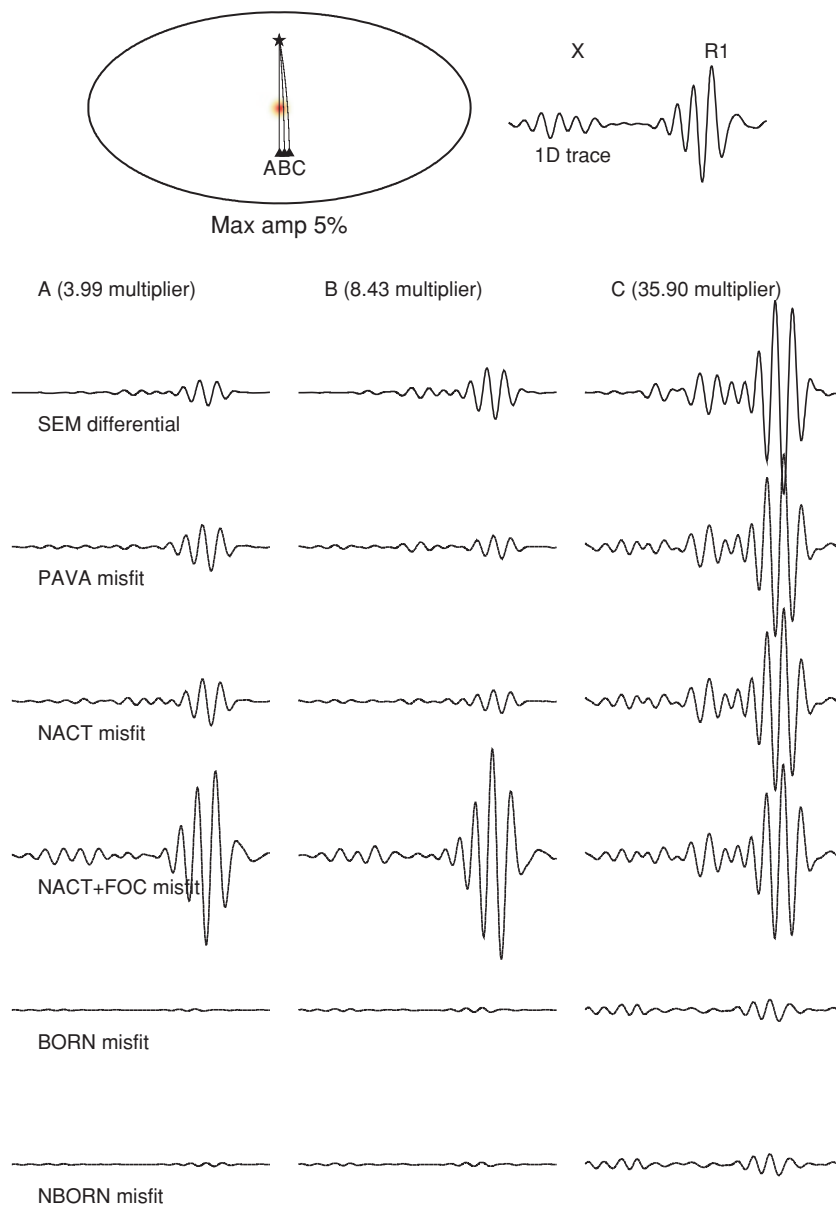
Figure 6. (*Continued.*)

the fundamental mode and the smaller overtone wave train. In this case, again, the asymptotic computation of focusing effects does an excellent job.

This example illustrates that: (1) the fundamental mode wave train is generally well explained by PAVA and (2) focusing effects are generally more important for the fundamental mode than 2-D effects in the vertical plane. Many papers have discussed the role of focusing in fundamental mode dispersion and waveform measurements (e.g. Spetzler *et al.* 2001; Yoshizawa & Kennett 2004; Zhou *et al.* 2004; Boschi 2006), however, we should stress that these discussions only apply to the case of isolated fundamental mode surface waves. As soon as overtones are considered, as shown in the previous section, the more important effect is the 2-D effect in the vertical plane.

Fig. 5 shows similar effects as Fig. 4, but this time at a larger distance (140° instead of 100°), where the asymptotic approximations are beginning to give less satisfactory results (they will eventually

break down near the antipode). Still, in the case of a path traversing through the middle of the anomaly (right-hand panel), PAVA is able to explain much of the 3-D effect, while the asymptotic focusing calculation 'overshoots', and predicts a larger than necessary perturbation in the fundamental mode. For a grazing path (left-hand panel), the asymptotic focusing computation provides a significant improvement over PAVA and NACT. However, it is necessary to perform the complete calculation of scattering over the surface of the sphere (i.e. BORN), in order to match the reference C-SEM differential (3D–1D) waveforms.

We note that this impressive BORN fit is obtained for a specific choice of size of anomaly. As discussed in Panning *et al.* (2008), the single scattering, linear, Born approximation breaks down for large amplitude, long wavelength anomalies, as it is not able to keep up with the monotonous accumulation of phase delay along the path, in which case it is important to include the multiple forward scattering, as proposed in the 'NBORN' formalism. Fig. 6(a) shows

an example comparing all the asymptotic approximations to the BORN and NBORN ones, for paths interacting with the single low velocity anomaly over different distances. While the largest misfits are for PAVA and NACT for the path just outside of the anomaly, these latter two approximations work much better for the path that travels through the centre of the large anomaly. Interestingly, in this particular case, the best fit is obtained in all cases for the NACT+FOC approximation. On the other hand, when the anomaly is of shorter wavelength, as shown in Fig. 6(b), BORN provides the best fits for all paths, and the NBORN approximation does not further improve the fits.

3.3 Domains of validity of various approximations

We have seen some simple examples illustrating the relative importance of 2-D effects in the vertical and horizontal planes for different parts of the seismogram. We showed these for specific geometries, and a specific size of heterogeneity, corresponding to a degree 16 term in a spherical harmonics expansion (i.e. a wavelength of about 1200 km, that is twice the wavelength of the shortest periods considered in our calculations). It is also instructive to compare the performance of the various approximations in a wider range of epicentral distances, azimuths, as well as sizes of anomalies. In what follows, we will consider anomalies of three different wavelengths, respectively with diameters of 5, 15 and 22.5°.

Fig. 7 compares residual variance plots for the fundamental mode Rayleigh wave, with respect to the 3-D C-SEM reference, for the four approximations (PAVA, NACT, NACT+FOC and BORN) in the case of a single low velocity anomaly of three different wavelengths. These comparison plots show that the BORN approximation works very well, as expected, for the case of the smallest anomaly, giving practically perfect fits to the reference C-SEM calculations. However, as the wavelength of the anomaly increases, the BORN fits deteriorate for paths traversing the anomaly. For the longest wavelength anomaly, BORN performs poorly along the paths that spend the most time inside the anomaly, and in that case, the asymptotic, but non-linear NACT+FOC approximation gives significantly better results than BORN. In the case of a single anomaly, results are practically the same for PAVA and NACT, regardless of the size of the anomaly, although for the larger anomalies, we can see an increasing misfit as we approach the antipode.

Fig. 8 shows the effects of the same geometries on the overtone wave packet. Here, all of the approximations work better in general, but we see a clear improvement of NACT over PAVA, especially near the axis of symmetry of the model and just beyond the anomaly, where 2-D effects in the vertical plane are the strongest. The BORN approximation works better for overtones than fundamental modes for all wavelengths of anomaly considered.

In Figs 9 and 10, we show the results for the two anomaly case, for the same three wavelengths of anomaly as in Figs 7 and 8. For the fundamental mode (Fig. 9) we see that there is little difference between the performance of PAVA and NACT, which reinforces the fact that PAVA is an excellent approximation for the isolated fundamental mode. There is little improvement when adding the asymptotic focusing, which performs poorly when the receiver is located in the area between the two anomalies, and at large distances in the case of the smallest wavelength anomaly. For the largest wavelengths anomalies, all the approximations perform equally, except in the region between the anomalies, where PAVA/NACT
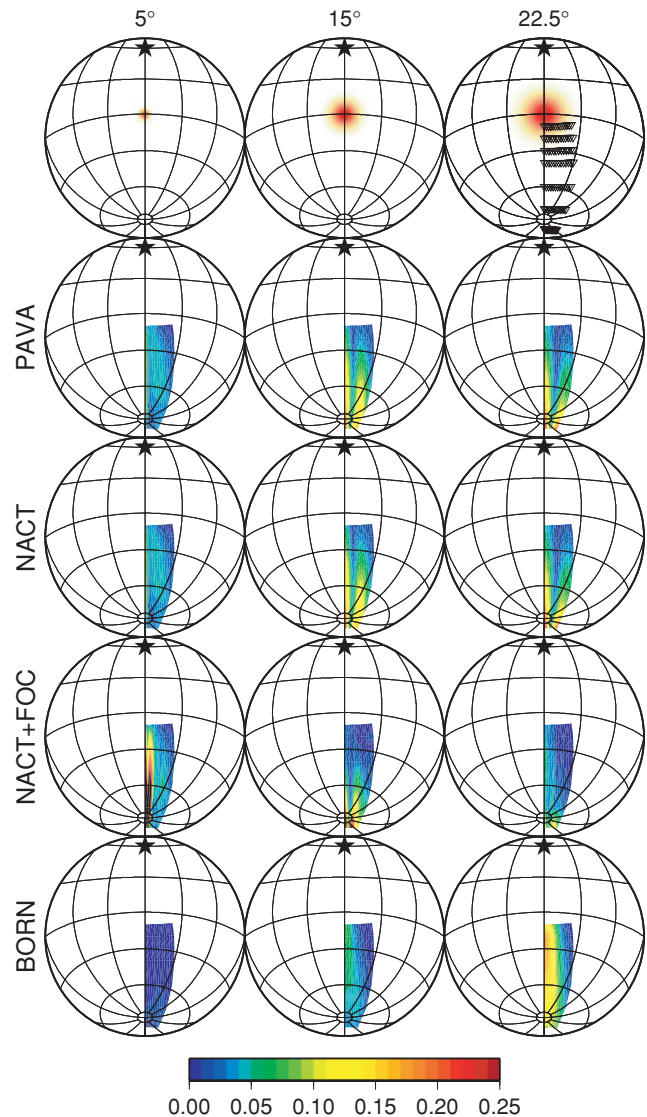

Figure 7. Comparison of RMS misfits to CSEM obtained using different approximations, for a range of azimuths and distances, and for 3 different sizes of single low velocity anomalies. The star denotes the location of the source. In this Fig. and the following, the misfit is defined as an RMS average of the difference between the approximate waveform and the 3-D SEM waveform, over the specified group velocity window, normalized by the RMS amplitude of the 3-D SEM trace of the same window. Here the misfit has been calculated for the fundamental mode only (group velocity window from 4.6 to 3.3 km s^{-1}). Left-hand panel: anomaly of diameter 5°; Middle panel: anomaly of diameter 15°; Right-hand panel: anomaly of diameter 22.5°. Only a small range of azimuths is shown, as the effects of the heterogeneous structure become insignificant for paths further away from the anomaly.

give the best results, and BORN performs very poorly. We see here another manifestation of the breakdown of BORN when sampling large wavelength anomalies: in this case the path only samples the first, fast anomaly. The phase shift accumulated on this path is too large to be explained by single scattering, while for longer paths, the opposite sign phase shift gradually compensates for it, and the BORN approximation eventually becomes more accurate again. The NACT+FOC approximation also breaks down in the region between the anomalies, most likely because of incomplete (divergent) account of the wave front healing effect.
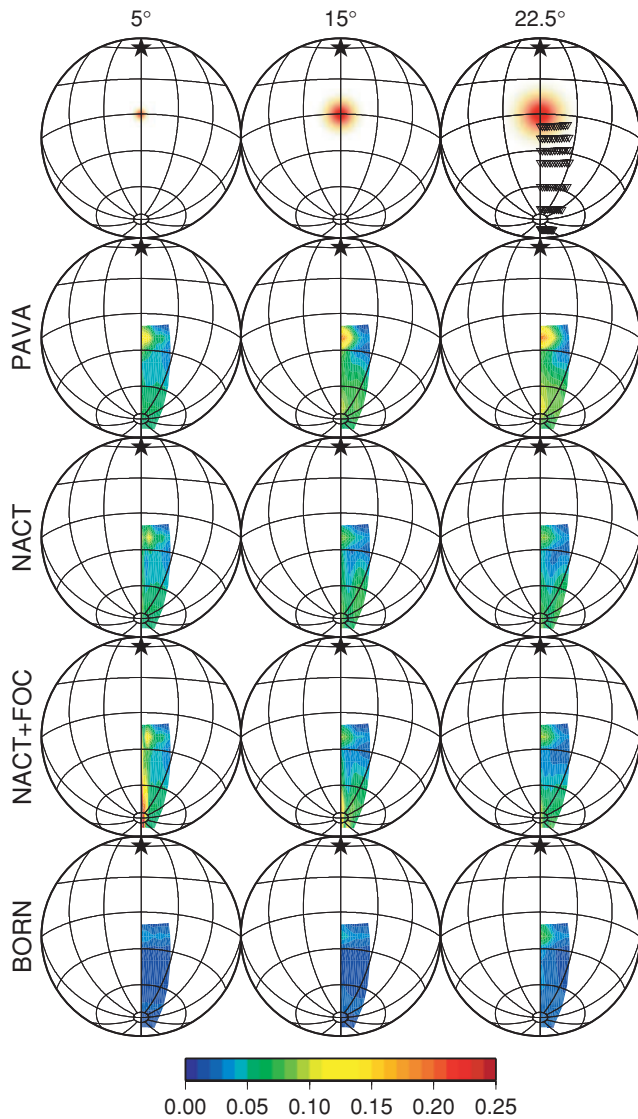
Figure 8. Same as Fig. 7, but now the misfit has been computed for the overtone and body wave portion of the seismograms (group velocity window 18.5–4.6 km s^{-1}).

Figure 9. Same as Fig. 7, but for the two anomaly case (Model 2) and a double couple source located on the equator. Here the misfit is computed for the fundamental mode wave packet.

linear BORN approximation with the non-linear forward scattering as expressed in PAVA is therefore our preferred approach in all cases (e.g. Panning *et al.* 2008).

In the case of overtones (Fig. 10), we again see the improvement of NACT over PAVA, especially for the larger wavelength anomalies, where the effect is quite strong. Adding asymptotic focusing does not help, and introduces large errors when the receiver is located between the two anomalies. For overtones, BORN works the best for all sizes of anomalies, as was previously found in the case of the single anomaly.

In summary, the synthetic tests presented indicate that:

(1) NACT works better than PAVA when the structure varies laterally in the vertical plane containing source and receiver.

(2) BORN works better than the asymptotic approximations at all wavelengths for overtones, although when the anomalies have large wavelengths, the difference with NACT is not very significant, considering the large amount of additional computations required.

(3) In the case of fundamental modes, however, BORN significantly outperforms the asymptotic computations only for small wavelength anomalies. When the anomalies are large, there are geometries in which BORN gives the poorest fits. Combining the
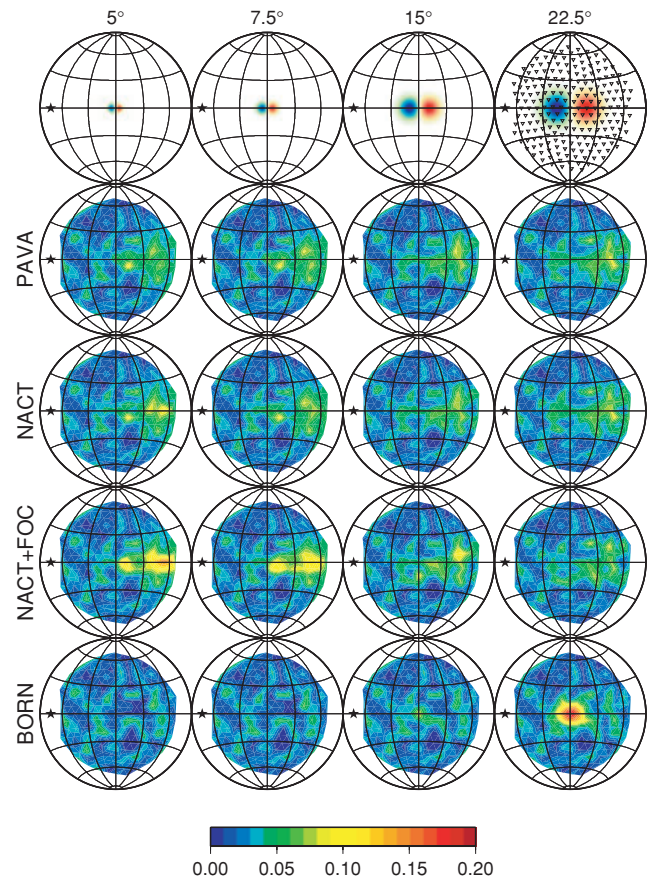
4 CONCLUSIONS

We have described and compared several approximations commonly used in modelling teleseismic wave propagation in a 3-D spherical earth, using as reference the 'exact' numerical CSEM computations. Our experiments illustrate that, when fundamental modes only are considered, 2-D effects in the horizontal plane (focusing) are more important than 2-D effects in the vertical plane. On the other hand, for overtone wave packets, the 2-D effects in the vertical plane need to be considered, while focusing effects are of secondary importance. The complete single scattering calculation (Born approximation) outperforms asymptotic approximations in the case of small wavelength anomalies (compared to the wavelength of the seismic waves considered), but in the case of long wavelength anomalies, the PAVA and NACT approximations give more accurate results because they can better account for the monotonic accumulation of phase shift along the path.

In the real earth, and particularly in the upper mantle, there are large provinces separated by sharp boundaries. Combining the advantages of the PAVA/NACT approach with those of an accurate single scattering calculation is therefore desirable, short of a complete numerical computation such as afforded by the SEM.
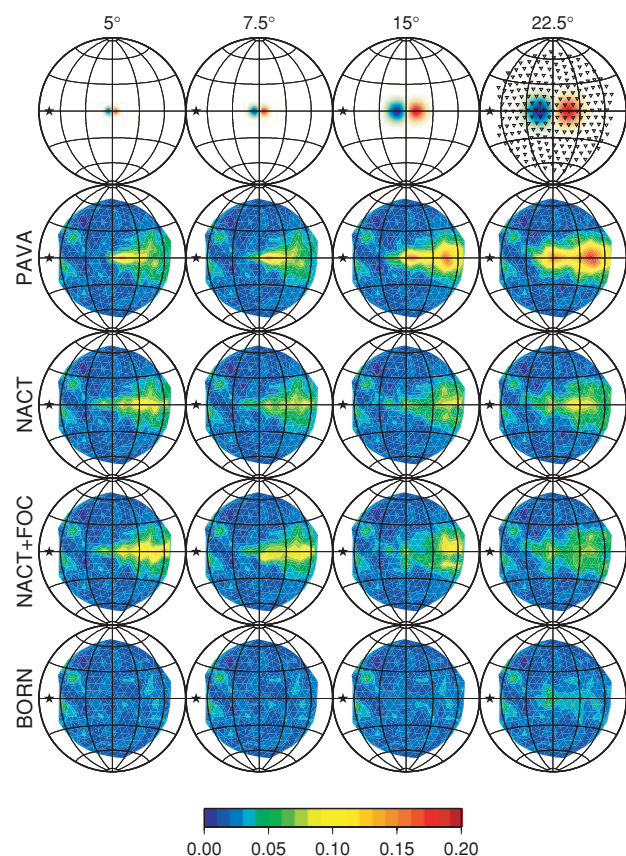
Figure 10. Same as Fig. 9, but the misfit is now computed for the overtone and body wave window.

REFERENCES

Andrews, J.A.D. & Woodhouse, J.H., 2006. Coupled normal-mode sensitivity to inner-core shear velocity and attenuation, *Geophys. J. Int.,* **167,** 204–212.

Boschi, L., 2006. Global multiresolution models of surface wave propagation: comparing equivalently regularized born and ray theoretical solutions, *Geophys. J. Int.,* **167,** 238–252.

Capdeville, Y., 2005. An efficient Born normal mode method to compute sensitivity kernels and synthetic seismograms in the earth, *Geophys. J. Int.,* **163**(2), 639–646.

Capdeville, Y., Chaljub, E., Vilotte, J. & Montagner, J., 2002. Coupling the spectral element method with a modal solution for elastic wave propagation in global Earth models, *Geophys. J. Int.,* **152,** 34–66.

Chaljub, E., Capdeville, Y. & Vilotte, J.-P., 2003. Solving elastodynamics in a fluid-solid heterogeneous sphere: a parallel spectral element approximation on non-conforming grids, *J. Comp. Phys.,* **187,** 457–491.

Chen, P., Jordan, T. & Zhao, L., 2007. Full three-dimensional tomography: a comparison between the scattering-integral and adjoint-wavefield methods, *Geophys. J. Int.,* **170,** 175–181.

Clévédé, E. & Lognonné, P., 1996. Frechet derivatives of coupled seismograms with respect to an anelastic rotating earth, *Geophys. J. Int.,* **124,** 456–482.

Clévédé, E., Mégnin, C., Romanowicz, B. & Lognonné, P., 2000. 'Modeling of waveforms in a 3-D Earth: asymptotic and non-asymptotic approaches', *P.E.P.I.,* **119,** 37–56.

Dahlen, F.A., 1968. The normal modes of a rotating, elliptical earth, *Geophys J. R. astr. Soc.,* **16,** 329–367.

Dahlen, F.A., Hung, S.H. & Nolet, G., 2000. Frechet kernels for finite-frequency traveltimes, I– theory, *Geophys. J. Int.,* **141,** 157–174.

Dalton, C.A. & Ekström, G., 2006. Constraints on global maps of phase velocity from surface-wave amplitudes, *Geophys. J. Int.,* **167,** 820–826.

Durek, J. & Romanowicz, B., 1999. Inner core anisotropy inferred by direct inversion of normal mode spectra, *Geophys. J. Int.,* **139,** 599–622.

Dziewonski, A. & Anderson, D.L., 1981. Preliminary Reference Earth Model, *Phys. Earth planet. Inter.,* **25,** 297–356.

Giardini, D., Li, X.-D. & Woodhouse, J.H., 1988. Splitting functions of long-period normal modes of the Earth, *J. geophys. Res.,* **93,** 13 716–13 742.

Gung, Y.C. & Romanowicz, B., 2004. Q tomography of the upper mantle using three component long period waveforms, *Geophys. J. Int.,* **157,** 813–830.

Jordan, T., 1978. Procedure for estimating lateral variations from low-frequency eigen-spectra data, *Geophys. J. R. astr. Soc.,* **52**(3), 441–455.

Komatitsch, D. & Tromp, J., 1999. Introduction to the spectral element method for three-dimensional seismic wave propagation, *Geophys. J. Int.,* **139,** 806–822.

Komatitsch, D. & Vilotte, J.P., 1998. The spectral element method: an effective tool to simulate the seismic response of 2D and 3D geological structures, *Bull. seism. Soc. Am.,* **88,** 368–392.

Kuo, C. & Romanowicz, B., 2002. On the resolution of density anomalies in the Earth's mantle using spectral fitting of normal mode data, *Geophys. J. Int.,* **150,** 162–179.

Lekic, V. & Romanowicz, B., 2007. Finite frequency upper mantle tomography using the Spectral Element Method, in *AGU Fall Meeting Suppl,* S32A–05.

Li, X.-D. & Romanowicz, B., 1995. Comparison of global waveform inversions with and without considering cross branch coupling, *Geophys. J. Int.,* **121,** 695–709.

Li, X.D. & Romanowicz, B., 1996. Global mantle shear velocity model developed using nonlinear asymptotic coupling theory, *J. geophys. Res.,* **101,** 22 245–22 273.

Li, X.D. & Tanimoto, T., 1993. Waveforms of long period body waves in a slightly aspherical earth, *Geophys. J. Int.,* **112,** 92–112.

Li, X.-D., Giardini, D. & Woodhouse, J.H., 1991. Large-scale three-dimensional even-degree structure of the Earth from splitting of long-period normal modes, *J. geophys. Res.,* **96,** 551–577.

Lognonné, P., 1991. Normal modes and seismograms in an anelastic rotating Earth, *J. geophys. Res.,* **96,** 20 309–20 319.

Lognonné, P. & Romanowicz, B., 1990. Fully coupled Earth's vibrations: the spectral method, *Geophys. J. Int.,* **102,** 365–395.

Masters, T.G., Jordan, T.H., Silver, P.G. & Gilbert, F., 1982. Aspherical Earth structure from fundamental speroidal-mode data, *Nature,* **298,** 609–613.

Mochizuki, E., 1986a. The free oscillations of an anisotropic and heterogeneous Earth, *Geophys. J. R. astr. Soc.,* **86,** 167–176.

Mochizuki, E., 1986b. Free oscillations and surface waves of an aspherical earth, *Geophys. Res. Lett.,* **13,** 1478–1481.

Montelli, R., Nolet, G., Dahlen, F., Masters, G., Engdahl, E. & Hung, S.-H., 2004. Finite-frequency tomography reveals a variety of plumes in the mantle, *Science,* **303**(5656), 338–343.

Nolet, G. & Dahlen, F.A., 2000. Wavefront hearling and the evolution of seismic delay times, *J. geophys. Res.* **105,** 19 043–19 054.

Panning, M., Capdeville, Y. & Romanowicz, B., 2008. Do first order 3D Born finite-frequency kernels improve modeling of surface waveforms?, *Geophys. J. Int.,* in press.

Park, J., 1987. Asymptotic coupled-mode expressions for multiplet amplitude anomalies and frequency shifts on an aspherical earth, *Geophys. J. Int.,* **90,** 129–169.

Phinney, R.A. & Burridge, R., 1972. Representation of the elastic-gravitational excitation of a spherical earth model by generalized spherical harmonics, *Geophys. J. Int.,* **34,** 451–487.

Pollitz, F., Park, J. & Dahlen, F.A., 1987. Observations of free oscillation amplitude anomalies *Geophys. Res. Lett.,* **14,** 895–898.

Resovsky, J.S. & Ritzwoller, M.H., 1995. Constraining odd-degree Earth

structure with coupled free-oscillations, *Geophys. Res. Lett.,* **16,** 2301–2304.

Romanowicz, B., 1987. Multiplet–multiplet coupling due to lateral heterogeneity: asymptotic effects on the amplitude and frequency of the Earth's normal modes, *Geophys. J. R. astr. Soc.,* **90,** 75–100.

Romanowicz, B., 2003. Global mantle tomography: progress status in the last 10 years, *Annu. Rev. Geophys. Space Phys.,* **31**(1), 303–328.

Romanowicz, B., 2008. Using seismic waves to image Earth's internal structure, *Nature,* **451,** 266–268.

Romanowicz, B. & Roult, G., 1986. First-order asymptotics for the eigenfrequencies of the Earth and application to the retrieval of large-scale lateral variations of structure, *Geophys. J. R. astr. Soc.,* **87**(1), 209–239.

Romanowicz, B. & Snieder, R., 1988. A new formalism for the effect of lateral heterogeneity on normal modes and surface waves II. General anisotropic perturbation, *Geophys. J. Int.,* **93,** 91–99.

Spetzler, J., Trampert, J. & Snieder, R., 2001. Are we exceeding the limits of the great circle approximation in global surface wave tomography? *Geophys. Res. Lett.,* **28**(12), 2341–2344.

Takeuchi, N., 2007. Whole mantle SH velocity model constrained by waveform inversion based on three dimensional Born kernels, *Geophys. J. Int.,* **169,** 1153–1163.

Tanimoto, T., 1984. A simple derivation of the formula to calculate synthetic long-period seismograms in a heterogeneous earth by normal mode summation, *Geophys. J. R. astr. Soc.,* **77,** 275–278.

Tanimoto, T., 1986. Free oscillations of a slightly anisotropic Earth, *Geophys. J. Int.,* **87,** 493–517.

Trampert, J. & Spetzler, J., 2006. Surface wave tomography: finite-frequency effects lost in the null space, *Geophys. J. Int.,* **164,** 394–400.

Tromp, J., Tape, C. & Liu, Q., 2005. Seismic tomography, adjoint methods, time reversal and banana-doughnut kernels, *Geophys. J.Int.,* **160,** 195–216.

Woodhouse, J.H., 1980. The coupling and attenuation of nearly resonant multiplets in the earth's free oscillation spectrum, *Geophys. J. R. astr. Soc.,* **61,** 261–283.

Woodhouse, J.H., 1983. The joint inversion of seismic wave forms for lateral variations in earth structure and earthquake source parameters, in *Earthqiakes: Observation, Theory and Interpretation,* Vol. 85, pp. 366–397, eds Kanamori, H. & Boschi, E., Proc. Int. School of Phys., Enrico Fermi.

Woodhouse, J.H. & Dahlen, F.A., 1978. The effect of a general aspherical perturbation on the free oscillations of the Earth, *Geophys. J. R. astr. Soc.,* **53,** 335–354.

Woodhouse, J. & Dziewonski, A., 1984. Mapping the upper mantle: three dimensional modeling of Earth structure by inversion of seismic waveforms, *J. geophys. Res.,* **89,** 5953–5986.

Woodhouse, J.H. & Girnius, T.P., 1982. Surface waves and free oscillations in a regionalized earth model, *Geophys. J. R. astr. Soc.,* **68,** 653–673.

Woodhouse, J.H. & Wong, Y., 1986. Amplitude, phase and path anomalies of mantle waves, *Geophys. J. R. astr. Soc.,* **87,** 753–773.

Yoshizawa, K. & Kennett, B., 2004. Multimode surface wave tomography for the Australian region using a three-stage approach incorporating finite frequency effects, *J. geophys. Res.,* **109,** doi:10.1029/2002JB002254.

Zhao, L., Jordan, T.H. & Chapman, C., 2000. Three-dimensional Fréchet differential kernels for seismic delay times, *Geophys. J. Int.,* **141,** 558–576.

Zhou, Y., Dahlen, F. & Nolet, G., 2004. Three-dimensional sensitivity kernels for surface wave observables, *Geophys. J. Int.,* **158,** 142–168.

APPENDIX:

We start by evaluating expression $A_{kk'}$ as defined in eqs (19) and (20): To order $1/l$, using the asymptotic expressions (28) for the normalized Legendre functions, we obtain:

$$
\begin{aligned}
A_{kk'} = \frac{1}{\pi^2} \sum_{NM} R_{kN} S_{k'M} \int_0^\pi \frac{\sin \lambda}{\sqrt{\sin \lambda}} \cos\left[k' F(k', M, \lambda)\right] \\
\times \int_0^{2\pi} g(\lambda, \mu) \cos\left[k F(k, N, \beta)\right] \\
\times \exp\left[i(M \Phi_{ps} - N \Phi_{pr})\right] \, d\lambda \, d\mu,
\end{aligned} \tag{A1}
$$

where

$$
kF(k, J, x) = kx - \frac{\pi}{4} + \frac{J\pi}{2} + \left(\frac{J^2}{2k} - \frac{1}{8k}\right) \cot x \tag{A2}
$$

and

$$
g(\lambda, \mu) = \frac{\delta \omega_{kk'}^2}{\sqrt{\sin \beta}} \exp\left[i(M \Phi_{ps} - N \Phi_{pr})\right]. \tag{A3}
$$

Let

$$
I(\lambda) = \int_0^{2\pi} g(\lambda, \mu) \cos\left[kF(\mu)\right] \, d\mu. \tag{A4}
$$

Then, following Romanowicz (1987), using the stationary phase approximation to order $1/l$:

$$
I(\lambda) = \sqrt{\frac{2\pi}{k|F_0''|}} \left[\cos\left(kF_0 + \frac{\pi}{4}\right) g_0 \right.
$$
$$
\left. - \frac{1}{k} \sin\left(kF_0 + \frac{\pi}{4}\right) \left(hg_0 + \frac{g_2}{2F_0''}\right) \right], \tag{A5}
$$

where the index '0' refers to computation of the corresponding function at $\mu = 0$ (i.e. on the great circle) and

$$
\begin{aligned}
\beta_0 &= \lambda - \Delta \\
kF_0 &= k\Delta - \frac{\pi}{4} + \frac{N\pi}{2} + \left(\frac{N^2}{2k} - \frac{1}{8k}\right) \cot \Delta \\
g_0 &= g(\lambda, 0) \\
\beta_0'' &= \frac{\partial^2 \beta}{\partial \mu^2}(\mu = 0) = \frac{\sin \lambda \sin \Delta}{\sin \beta_0} \\
g_2 &= \frac{\partial^2 g}{\partial \mu^2}(\mu = 0) \\
h &= -\frac{1}{8} \frac{F''''}{(\beta'')^2} = \frac{1}{8}\left[\frac{1}{\beta_0''} + 3 \cot \beta_0\right],
\end{aligned} \tag{A6}
$$

where $F'''' = \frac{\partial^4 F}{\partial \mu^4}$. After some algebra, g_2 becomes

$$
\begin{aligned}
g_2 = \frac{1}{\sqrt{\sin \beta_0}} \left[\frac{\partial^2 \delta \omega_{kk'}^2}{\partial \mu^2} - \frac{\delta \omega_{kk'}^2}{2} \beta_0'' \cot \beta_0 \right. \\
- \left(M - N \frac{\partial \mu'}{\partial \mu}|_0\right)^2 \delta \omega_{kk'}^2 \\
\left. + 2i \left(M - N \frac{\partial \mu'}{\partial \mu}|_0\right) \frac{\partial \delta \omega_{kk'}^2}{\partial \mu} \right],
\end{aligned} \tag{A7}
$$

where all quantities are calculated at $\mu = 0$.

Using the following relations in the configuration of Fig. 1

$$
\begin{aligned}
\Phi_{ps}|_0 &= \mu|_0 = 0 \\
\Phi_{pr}|_0 &= \mu'|_0 = \pi \\
\beta''_0 &= \frac{\sin \lambda \sin \Delta}{\sin \beta_0}
\end{aligned} \tag{A8}
$$

$$
\begin{aligned}
\cot \Delta &= \cot \lambda + \frac{1}{\beta_0''} \\
\frac{\partial \mu'}{\partial \mu}|_0 &= \frac{\sin \lambda}{\sin \beta_0}.
\end{aligned} \tag{A9}
$$

After some algebra, ignoring terms of order higher than $1/l$ and rapidly varying terms in $\cos(k\lambda)$, and assuming $\delta \omega_{kk'} = \delta \omega_{k'k} =$

$\delta\omega_{kk}$ (Romanowicz 1987), we obtain:

$$A_{kk'} = \frac{1}{2\pi^2}\sqrt{\frac{2\pi}{k}}\sum_{NM} R_{kN}S_{k'M} \cdot$$

$$2\omega_k \int_0^\pi d\lambda \left\{ \delta\omega_{kk}\cos[\Psi(\lambda)] + \frac{1}{2k}Q(\lambda, \delta\omega_{kk})\sin[\Psi(\lambda)] \right\}$$

$$\times \exp(-iN\pi), \tag{A10}$$

where

$$\Psi(\lambda) = k\Delta + n\lambda - \frac{\pi}{4} + (M-N)\frac{\pi}{2} \tag{A11}$$
$$n = l - l'$$

$$Q(\lambda, \delta\omega_{kk}) = \delta\omega_{kk}\left[\left(-\frac{M^2+N^2}{2} + \frac{1}{8}\right)\cot\Delta + \frac{MN}{\sin\Delta}\right]$$

$$+ i(ME_k^1 - NE_k^2) + \frac{1}{2}D_k \tag{A12}$$

with

$$E_k^1 = \frac{1}{\beta''_0}\frac{\partial\delta\omega_{kk}^2}{\partial\mu}$$

$$E_k^2 = \frac{1}{\beta''_0}\frac{\sin\lambda}{\sin\beta_0}\frac{\partial\delta\omega_{kk}^2}{\partial\mu} \tag{A13}$$

$$D_k = \frac{1}{2\beta''_0}\frac{\partial^2\delta\omega_{kk}}{\partial\mu^2}$$

so that

$$A_{kk'} = \frac{1}{2\pi^2}\sqrt{\frac{2\pi}{k}}\sum_{NM} R_{kN}S_{k'M}i^{N+M}2\omega_k \cdot$$

$$\int_0^\pi d\lambda \left\{ \delta\omega_{kk}\cos[\Psi_1(\lambda)] + \frac{1}{2k}Q(\lambda, \delta\omega_{kk})\sin[\Psi_1(\lambda)] \right\}, \tag{A14}$$

where

$$\Psi_1(\lambda) = k\Delta + n\lambda - \frac{\pi}{4} + (M+N)\frac{\pi}{2}$$
$$\cos(\Psi_1) = \exp(-iN\pi)\cos(\Psi) \tag{A15}$$
$$\sin(\Psi_1) = \exp(-iN\pi)\sin(\Psi)$$

and

$$Q(\lambda, \delta\omega_{kk}) = \delta\omega_{kk}\left[\left(-\frac{M^2+N^2}{2} + \frac{1}{8}\right)\cot\Delta + \frac{MN}{\sin\Delta}\right]$$

$$+ i\left(ME_k^1 - NE_k^2\right) + \frac{1}{2}D_k. \tag{A16}$$

Similarly

$$A_{k'k} = \frac{1}{2\pi^2}\sqrt{\frac{2\pi}{k}}\sum_{NM} R_{kN}S_{k'M}i^{N+M}$$

$$\times 2\omega_k \int_0^\pi d\lambda \left\{ \delta\omega_{kk}\cos[\Psi_2(\lambda)] + \frac{1}{2k}Q(\lambda, \delta\omega_{kk})\sin[\Psi_2(\lambda)] \right\}, \tag{A17}$$

where

$$\Psi_2(\lambda) = k\Delta - n(\lambda - \Delta) - \frac{\pi}{4} + (M+N)\frac{\pi}{2}. \tag{A18}$$

In order to obtain the complete seismogram, we now need to compute sums over modes: an across-branch coupling sum:

$\sum_{k'C\Gamma_k}\frac{(A_{kk'}+A_{k'k})}{\omega_k^2 - \omega_{k'}^2}$ and a self-coupling sum $\frac{\sum_k A_{kk}}{\omega_k}$ (eq. 21). The summation over k and k' can be replaced by summation over n, following the derivation of Romanowicz (1987), and noting that:

$$\omega_k^2 - \omega_{k+n}^2 \sim 2n\omega_k\frac{U}{a}, \tag{A19}$$

where U is group velocity of the multiplet k in the reference spherically symmetric earth. We find that the across-branch coupling sum can be expressed in terms of minor and great circle averages of the quantities defined in eq. (A13), and those of the local frequency $\delta\omega_{kk}$. On the other hand, the self-coupling sum can be expressed in terms of great circle averages of the same quantities.

From this, we readily obtain the following *linear* approximation to the seismogram, to order $1/l$:

$$u_k(t) = Re\sqrt{\frac{2\pi}{k}}\frac{1}{\pi\sqrt{\sin\Delta}}\exp(i\omega_k t - i\alpha_k t)\sum_{NM} i^{M+N}R_k^N S_k^M$$

$$\times \left\{ \cos\left[f_k(M,N) + \frac{\alpha_{NM}}{k}\right] \right.$$

$$+ it\left(\delta\hat{\omega}_{kk}\cos[f_k(M,N)] + \frac{Y_k}{k}\sin[f_k(M,N)]\right)$$

$$+ \frac{a\Delta}{U}\left([\delta\tilde{\omega}_{kk} - \delta\hat{\omega}_{kk}]\sin[f_k(M,N)]\right.$$

$$\left.\left. + \frac{X_k}{k}\cos[f_k(M,N)]\right)\right\}. \tag{A20}$$

Where we have defined

$$Y_k = Y_{kr} + iY_{ki}$$

$$= \frac{\hat{D}_k}{2} + \delta\hat{\omega}_{kk}\left[\frac{\cot\Delta}{8} + \frac{MN}{\sin\Delta} - \frac{\cot\Delta}{2}(M^2+N^2)\right]$$

$$+ i\left(M\hat{E}_k^1 - N\hat{E}_k^2\right)$$

$$X_k = X_{kr} + iX_{ki}$$

$$= \frac{\hat{D}_k - \tilde{D}_k}{2} + (\delta\hat{\omega}_{kk} - \delta\tilde{\omega}_{kk})\left[\frac{\cot\Delta}{8} + \frac{MN}{\sin\Delta}\right.$$

$$\left. - \frac{\cot\Delta}{2}(M^2+N^2)\right]$$

$$+ i\left[M(\hat{E}_k^1 - \tilde{E}_k^1) - N(\hat{E}_k^2 - \tilde{E}_k^2)\right]$$

$$f_k(M,N) = k\Delta - \frac{\pi}{4} + (M+N)\frac{\pi}{2}$$

$$\alpha_K^{NM} = \left(\frac{M^2+N^2}{2} - \frac{1}{8}\right)\cot\Delta - \frac{MN}{\sin\Delta} \tag{A21}$$

with the following definition of great circle and minor arc averages

$$\delta\tilde{\omega}_k = \frac{1}{\Delta}\int_0^\Delta \delta\omega_k(s)\,ds$$

$$\delta\hat{\omega}_k = \frac{1}{2\pi}\int_0^{2\pi} \delta\omega_k(s)\,ds$$

$$\delta\hat{D}_k = \frac{1}{2\pi}\int_0^{2\pi} D_k(s)\,ds$$

$$\delta\tilde{D}_k = \frac{1}{\Delta}\int_0^\Delta \delta D_k(s)\,ds \tag{A22}$$

$$\hat{E}_k^1 = \frac{1}{2\pi} \int_0^{2\pi} E_k^1(s)\,ds$$

$$\tilde{E}_k^1 = \frac{1}{\Delta} \int_0^{\Delta} E_k^1(s)\,ds$$

$$\hat{E}_k^2 = \frac{1}{2\pi} \int_0^{2\pi} E_k^2(s)\,ds$$

$$\tilde{E}_k^2 = \frac{1}{\Delta} \int_0^{\Delta} E_k^2(s)\,ds. \tag{A23}$$

The last step in obtaining expressions (45) and (46) involves performing the summations on N and M in eqs (A20). Here we develop eq. (A20) by separating, on the one hand, the Δ dependence [terms in $\cos(k\Delta - \pi/4)$ and $\sin(k\Delta - \pi/4)$], and on the other, zeroth order terms from order $(1/l)$ terms. For this it is useful to define the following quantities:

$$T_0 = \sum_{NM} R_k^N S_k^M i^{M+N} \cos(M+N)\pi/2$$

$$T_1 = \sum_{NM} R_k^N S_k^M i^{M+N} \sin(M+N)\pi/2$$

$$F_1 = \sum_{NM} R_k^N S_k^M i^{M+N} X_{Kr}^{NM} \cos(M+N)\pi/2$$

$$F_2 = \sum_{NM} R_k^N S_k^M i^{M+N} X_{Kr}^{NM} \sin(M+N)\pi/2$$

$$F_3 = \sum_{NM} R_k^N S_k^M i^{M+N} Y_{Kr}^{NM} \cos(M+N)\pi/2$$

$$F_4 = \sum_{NM} R_k^N S_k^M i^{M+N} Y_{Kr}^{NM} \sin(M+N)\pi/2$$

$$F_5 = \sum_{NM} R_k^N S_k^M i^{M+N} \alpha_K^{NM} \cos(M+N)\pi/2$$

$$F_6 = \sum_{NM} R_k^N S_k^M i^{M+N} \alpha_K^{NM} \sin(M+N)\pi/2$$

$$i\tilde{F}_7 = \sum_{NM} R_k^N S_k^M i^{M+N} X_{Ki}^{NM} \cos(M+N)\pi/2$$

$$i\tilde{F}_8 = \sum_{NM} R_k^N S_k^M i^{M+N} X_{Ki}^{NM} \sin(M+N)\pi/2$$

$$i\tilde{F}_9 = \sum_{NM} R_k^N S_k^M i^{M+N} Y_{Ki}^{NM} \cos(M+N)\pi/2$$

$$i\tilde{F}_{10} = \sum_{NM} R_k^N S_k^M i^{M+N} Y_{Ki}^{NM} \sin(M+N)\pi/2, \tag{A24}$$

where the quantities Y and X have been defined in eq. (A21).

Using expressions (A24), eq. (A20) then becomes:

$$u_k(t, \Delta) = \frac{1}{\pi k_l \sqrt{\sin \Delta}} \left[\cos\left(k\Delta - \frac{\pi}{4}\right)(B_0 \cos\omega_k t - t B_1 \sin\omega_k t) \right.$$
$$\left. + \sin\left(k\Delta - \frac{\pi}{4}\right)(C_0 \cos\omega_k t - t C_1 \sin\omega_k t) \right], \quad \text{(A25)}$$

where

$$B_0 = T_0 + \frac{a\Delta}{kU}(F_1 - \tilde{F}_7) - \frac{F_6}{k} + \frac{a\Delta}{U}(\delta\tilde{\omega}_k - \delta\hat{\omega}_k) T_1$$

$$B_1 = T_0 \delta\hat{\omega}_k + \frac{F_4 - \tilde{F}_{10}}{k}$$

$$C_0 = -T_1 - \frac{a\Delta}{kU}(F_2 - \tilde{F}_8) - \frac{F_5}{k} + \frac{a\Delta}{U}(\delta\tilde{\omega}_k - \delta\hat{\omega}_k) T_0$$

$$C_1 = -T_1 \delta\hat{\omega}_k + \frac{F_3 - \tilde{F}_9}{k}. \tag{A26}$$

To obtain eq. (45), we drop the zeroth order terms, since, in practice, we replace those with the non-linear PAVA approximation.

Expressions (A24) can be further evaluated as follows. Using the expressions in table 1 of Woodhouse & Girnius (1982), we define:

$$\tilde{R}_0 = R_0 = k_0 U v_r$$

$$\tilde{R}_1 = i(R_{-1} + R_1) = 2k_1(V v_\phi + W v_\theta)$$

$$\tilde{S}_0 = S_0 = -k_0 \left[\partial_r U M_{rr} + \frac{1}{2} f(M_{\theta\theta} + M_{\phi\phi}) \right]$$

$$\tilde{S}_1 = -i(S_1 + S_{-1}) = -2k_1(Z M_{r\theta} + X M_{r\phi})$$

$$\tilde{S}_2 = S_2 + S_{-2} = -2\frac{k_2}{r_s} \left[V(M_{\theta\theta} - M_{\phi\phi}) - 2W M_{\theta\phi} \right]$$

$$\tilde{R}_{-1} = R_1 - R_{-1} = 2k_1(V v_\theta + W v_\phi)$$

$$\tilde{S}_{-1} = S_1 - S_{-1} = 2k_1(Z M_{r\phi} - X M_{r\theta}) \tag{A27}$$

$$\tilde{S}_{-2} = i(S_2 - S_{-2}) = -2\frac{k_2}{r_s} \left[2V M_{\theta\phi} + W(M_{\theta\theta} - M_{\phi\phi}) \right],$$

where v_r, v_θ, v_ϕ are the components of the instrument vector and

$$f = \frac{2U - l(l+1)V}{r}$$

$$X = \partial_r V + \frac{U - V}{r}$$

$$Z = \partial_r W - \frac{W}{r}. \tag{A28}$$

Note that all quantities named $\tilde{S}$ are evaluated at the source depth r_s, while all quantities named $\tilde{R}$ are evaluated at the earth's surface $r = a$.

Then:

$$T_0 = \tilde{R}_1 \tilde{S}_1 + \tilde{R}_0(\tilde{S}_0 + \tilde{S}_2)$$

$$T_1 = \tilde{R}_1(\tilde{S}_0 + \tilde{S}_2) - \tilde{R}_0 \tilde{S}_1$$

$$F_1 = a_{01} \left[\tilde{R}_1 \tilde{S}_1 + \tilde{R}_0(\tilde{S}_0 + \tilde{S}_2) \right]$$
$$\quad + a_{11} \tilde{R}_{-1} S_{-1} + a_{21} \left[\tilde{R}_1 \tilde{S}_1 + 2\tilde{S}_2 \tilde{R}_0 \right]$$

$$F_2 = a_{01} \left[\tilde{R}_1(\tilde{S}_2 + \tilde{S}_0) - \tilde{R}_0 \tilde{S}_1 \right]$$
$$\quad + \frac{a_{21}}{2} \left[\tilde{R}_0 \tilde{S}_1 - \tilde{R}_1 \tilde{S}_0 - 5\tilde{R}_1 \tilde{S}_2 \right] + 2a_{11} \tilde{R}_{-1} \tilde{S}_{-2}$$

$$F_3 = a_{02} \left[\tilde{R}_1 \tilde{S}_1 + \tilde{R}_0(\tilde{S}_0 + \tilde{S}_2) \right]$$
$$\quad + a_{12} \tilde{R}_{-1} S_{-1} + a_{22} \left[\tilde{R}_1 \tilde{S}_1 + 2\tilde{S}_2 \tilde{R}_0 \right]$$

$$F_4 = a_{02} \left[\tilde{R}_1(\tilde{S}_2 + \tilde{S}_0) - \tilde{R}_0 \tilde{S}_1 \right]$$
$$\quad + \frac{a_{22}}{2} \left[\tilde{R}_0 \tilde{S}_1 - \tilde{R}_1 \tilde{S}_0 - 5\tilde{R}_1 \tilde{S}_2 \right] + 2a_{12} \tilde{R}_{-1} \tilde{S}_{-2}$$

$$F_5 = a_{03} \left[\tilde{R}_1 \tilde{S}_1 + \tilde{R}_0(\tilde{S}_0 + \tilde{S}_2) \right]$$
$$\quad + a_{13} \tilde{R}_{-1} S_{-1} + a_{23} \left[\tilde{R}_1 \tilde{S}_1 + 2\tilde{S}_2 \tilde{R}_0 \right]$$

$$F_6 = a_{03} \left[\tilde{R}_1(\tilde{S}_2 + \tilde{S}_0) - \tilde{R}_0 \tilde{S}_1 \right]$$
$$\quad + \frac{a_{23}}{2} \left[\tilde{R}_0 \tilde{S}_1 - \tilde{R}_1 \tilde{S}_0 - 5\tilde{R}_1 \tilde{S}_2 \right] + 2a_{13} \tilde{R}_{-1} \tilde{S}_{-2}$$

$$\tilde{F}_7 = -a_{31} \left[\tilde{R}_1 \tilde{S}_{-1} + 2\tilde{R}_0 \tilde{S}_{-2} \right] - a_{41} \tilde{R}_{-1} \tilde{S}_1$$

$$\tilde{F}_8 = -a_{31} \left[2\tilde{S}_{-2} \tilde{R}_1 - \tilde{R}_0 \tilde{S}_{-1} \right] - a_{41} \left[\tilde{R}_{-1}(\tilde{S}_0 + \tilde{S}_2) \right]$$

$$\tilde{F}_9 = -a_{32} \left[\tilde{R}_1 \tilde{S}_{-1} + 2\tilde{R}_0 \tilde{S}_{-2} \right] - a_{42} \tilde{R}_{-1} \tilde{S}_1$$

$$\tilde{F}_{10} = -a_{32} \left[2\tilde{S}_{-2} \tilde{R}_1 - \tilde{R}_0 \tilde{S}_{-1} \right] - a_{42} \left[\tilde{R}_{-1}(\tilde{S}_0 + \tilde{S}_2) \right] \tag{A29}$$

with

$$a_{01} = \frac{\hat{D}_k - \tilde{D}_k}{2} + \frac{\cot \Delta}{8} (\delta \hat{\omega}_k - \delta \tilde{\omega}_k)$$

$$a_{11} = \frac{\delta \hat{\omega}_k - \delta \tilde{\omega}_k}{\sin \Delta}$$

$$a_{21} = (\delta \hat{\omega}_k - \delta \tilde{\omega}_k) \cot \Delta$$

$$a_{02} = \frac{\hat{D}_k}{2} + \frac{\cot \Delta}{8} \delta \hat{\omega}_k$$

$$a_{12} = \frac{\delta \hat{\omega}_k}{\sin \Delta}$$

$$a_{22} = \delta \hat{\omega}_k \cot \Delta$$

$$a_{03} = -\frac{\cot \Delta}{8}$$

$$a_{13} = -\frac{1}{\sin \Delta}$$

$$a_{23} = -\cot \Delta$$

$$a_{31} = \hat{E}_k^1 - \tilde{E}_k^1$$

$$a_{32} = \hat{E}_k^1$$

$$a_{41} = \hat{E}_k^2 - \tilde{E}_k^2$$

$$a_{42} = \hat{E}_k^2. \tag{A30}$$